Electron and neutrino scattering off the deuteron in a relativistic framework

A. Grassi,[1] J. Golak,[1] W. N. Polyzou,[2] R. Skibiński,[1] H. Witała,[1] and H. Kamada[3]

[1] *M. Smoluchowski Institute of Physics, Jagiellonian University, PL-30348 Kraków, Poland*

[2] *Department of Physics and Astronomy, The University of Iowa, Iowa City, Iowa 52242, USA*

[3] *Department of Physics, Faculty of Engineering, Kyushu Institute of Technology, Kitakyushu 804-8550, Japan*

(Dated: November 4, 2022)

Abstract

We build a relativistic model to perform calculations of exclusive, semi-exclusive and inclusive unpolarized cross sections and various polarization observables in electron and neutrino scattering experiments with deuteron targets. The strong interaction dynamics is defined by an explicit dynamical unitary representation of the Poincaré group, where representations of space translations and rotations in the interacting and non-interacting representations are the same. The Argonne V18 potential is used to construct a relativistic nucleon-nucleon interaction reproducing the experimental deuteron binding energy and nucleon-nucleon scattering observables. Our formalism does not include the pion production channel and neglects two-body contributions in the electromagnetic as well as in the weak nuclear current operator. We show that it is applicable to processes at kinematics, where the internal two-nucleon energy remains below the pion production threshold but the magnitude of the three-momentum transfer extends at least to several GeV.

I. INTRODUCTION

The deuteron is the simplest bound system of nucleons. Because of its simplicity it is an ideal system for detailed investigations of strong interaction dynamics. The deuteron can be modeled in terms of experimentally observable particle degrees of freedom or in terms of sub-nucleon degrees of freedom. As long as the energy scale is limited, both representations can in principle be used to calculate the same experimentally observable scattering matrix. Understanding the relation between these two representations is a central question in nuclear physics applications. One of the most useful ways to study the dynamics and structure of the deuteron is by scattering deuterons with photons, electrons or neutrinos. This is because the scattering reaction can be accurately approximated in the lowest non-trivial order in the electroweak interaction. In this approximation the scattering operator is linear in the hadronic matrix elements of hadronic current operators. The hadronic current operators encode the density and motion of the strongly interacting charged constituent particles. The representation of the hadronic current is largely determined by the representation of the interaction. In the coordinate representation a locally gauge invariant Hamiltonian can be constructed by replacing momentum operators in the Hamiltonian by gauge covariant derivatives. The current is the coefficient of the part of the gauge invariant Hamiltonian that is linear in the vector potential. In general it has a cluster expansion which is a sum of

interaction-independent one-body and interaction-dependent many-body operators.

In a scattering experiment involving electroweak probes the initial and final hadronic states are in different frames related by the momentum transferred to the target deuteron by the electron, photon or neutrino. Probes with sufficient resolution to be sensitive to sub-nucleon degrees of freedom must have high momentum transfers which require a relativistic description of the strong interaction dynamics.

The most detailed information about the hadronic current is contained in exclusive spin-dependent matrix elements of the current. Calculations using realistic interactions with controlled approximations are possible for spin-dependent elastic scattering and breakup reaction observables. The available phase space that can be explored is large and comparison of detailed computations with experiment can put strong constraints on the model interactions, which have implications for larger nuclei. The deuteron is also a special system because quasi-elastic scattering off deuteron targets supplies important information about electroweak scattering from neutrons.

The purpose of this work is to develop tools to perform consistent relativistic calculations of spin-dependent observables in electroweak scattering experiments on deuteron targets. In this work the strong interaction dynamics is defined by an explicit dynamical unitary representation of the Poincaré group [1]. The dynamical Poincaré generators are constructed using a relativistic re-interpretation [2] of the Argonne V18 interaction [3] that is designed to reproduce the experimentally observable deuteron binding energy and nucleon-nucleon scattering observables. The dynamical representation is chosen so representations of space translations and rotations are identical in the interacting and non-interacting representations [4]. The focus in this work is on the spin-dependent observables in elastic and inelastic scattering from deuterons.

The scope of this work is limited in two ways. First, a pion production channel is not included. The second limitation is that the dynamical two-body contributions to the current that arise from local gauge invariance are not taken into account, although current covariance and current conservation can be satisfied by using the Wigner-Eckart theorem for the Poincaré group. The model can be extended to overcome both of these limitations. A realistic treatment of production reactions would require developing new nucleon-nucleon and production interactions that are consistent with nucleon-nucleon scattering data both above and below the pion production threshold. While a consistent derivation of two-body

currents is possible; ignoring them can be used to determine which reactions are sensitive to the dynamical parts of the current. These limitations, which require additional development, can be addressed in subsequent investigations. The present investigation should provide some clarity on which observables are sensitive to both two-body currents and/or production channels.

The next section discusses the structure of the theory, including the construction of the dynamical unitary representation of the Poincaré group. It also discusses the assumptions that are needed to justify the approximations used in the subsequent sections. Section III describes relativistic and non-relativistic kinematic relations that are used in the calculations. Results of numerical calculations for unpolarized cross sections and spin dependent observables are shown in Sec. IV. The summary and conclusions follow in Sec. V. Appendix A discusses the construction of nuclear current matrix elements in this formalism.

II. THEORY

In this work a relativistically invariant quantum mechanical model is defined by a unitary representation, $U(\Lambda, a)$, of the Poincaré group acting on the Hilbert space of the theory. This ensures that quantum observables (probabilities, expectation values and ensemble averages) are independent of the choice of inertial reference frame [1].

The dynamics is solved by simultaneously diagonalizing the mass and spin Casimir operators. This decomposes $U(\Lambda, a)$ into a direct integral of irreducible representations. This is the relativistic analog of diagonalizing the non-relativistic center of mass Hamiltonian.

The model Hilbert space is a multi-particle space determined by the particle content of the reaction. In this work the particles of the model are nucleons and leptons. Single-particle Hilbert spaces $\mathcal{H}_i$ are represented by square integrable functions of the particle's linear momentum and magnetic quantum numbers:

$$\langle\psi|\psi\rangle := \sum_{\mu=-j}^{j} \int |\langle(m,s)\mathbf{p},\mu|\psi\rangle|^2 d\mathbf{p} = 1. \tag{1}$$

Unless otherwise mentioned the non-covariant normalization above is assumed.

There are single-particle unitary representations of the Poincaré group, $U_k(\Lambda, a)$, that act on each $\mathcal{H}_k$. The representation determines the interpretation of the magnetic quantum numbers. For a particle of mass m and spin j a single-particle unitary representation of the

Poincaré group is defined on the single particle basis by

$$U(\Lambda,a)|(m,j)\mathbf{p},\mu\rangle =$$
$$e^{-ip'\cdot a}\sum_{\nu=-j}^{j}|(m,j)\mathbf{p}',\nu\rangle\sqrt{\frac{E(\mathbf{p}')}{E(\mathbf{p})}}\,D^{j}_{\mu\nu}[R_w(\Lambda,p)], \tag{2}$$

where

$$E(\mathbf{p})=\sqrt{m^2+\mathbf{p}^2} \tag{3}$$

is the particle's energy,

$$p'^{\mu}:=\Lambda^{\mu}{}_{\nu}p^{\nu} \tag{4}$$

is the transformed four momentum,

$$R_w(\Lambda,p):=B^{-1}(\mathbf{p}'/m)\Lambda B(\mathbf{p}/m) \tag{5}$$

is a $SU(2)$ Wigner rotation and $B(\mathbf{p}/m)^{\mu}{}_{\nu}$ is a rotationless Lorentz transformation that maps $(m,0,0,0)$ to $(E(\mathbf{p}),\mathbf{p})$:

$$B(\mathbf{p}/m)^{0}{}_{0}=E(\mathbf{p})/m,\qquad B(\mathbf{p}/m)^{i}{}_{0}=B(\mathbf{p}/m)^{0}{}_{i}=p^{i}/m, \tag{6}$$

$$B(\mathbf{p}/m)^{i}{}_{j}=\delta^{ij}+p^{i}p^{j}/(m(m+E(\mathbf{p}))). \tag{7}$$

In representation (2) the spin observable in an arbitrary frame is defined as the spin that would be measured in the particle's rest frame if it was boosted to the rest frame using $B^{-1}(\mathbf{p}/m)$. The $SL(2,C)$ version of $B(\mathbf{p}/m)$, which appears in the Wigner D-function, is $e^{\boldsymbol{\rho}\cdot\boldsymbol{\sigma}/2}$, where $\boldsymbol{\rho}$ is the rapidity of the boost and $\boldsymbol{\sigma}$ are the Pauli matrices.

The multi-particle Hilbert space is the tensor product of suitably symmetrized single-particle Hilbert spaces:

$$\mathcal{H}=\otimes_i\mathcal{H}_i. \tag{8}$$

The free dynamics on $\mathcal{H}$ is given by the tensor product of the single particle unitary representations, $U_i(\Lambda,a)$, of the Poincaré group

$$U_0(\Lambda,a)=\otimes_i U_i(\Lambda,a). \tag{9}$$

The infinitesimal generators of $U_0(\Lambda,a)$ are the free four momentum $P_0^{\mu}:=\sum_i P_{0i}^{\mu}$ and the free Lorentz generators $J_0^{\mu\nu}:=\sum_i J_{0i}^{\mu\nu}$. The free mass Casimir operator and canonical spin operators are functions of the infinitesimal generators of $U_0(\Lambda,a)$:

$$M_0=\sqrt{g_{\mu\nu}P_0^{\mu}P_0^{\nu}} \tag{10}$$

and

$$\mathbf{j}_0^k = \frac{1}{2}\epsilon^{ijk}B^{-1}(\mathbf{P_0}/M_0)^i{}_\mu B^{-1}(\mathbf{P_0}/M_0)^j{}_\nu J_0^{\mu\nu} \tag{11}$$

where in (11) $B(\mathbf{P_0}/M_0)^\mu{}_\nu$ is a canonical boost,(6)-(7), valued matrix of the operators P_0^μ/M_0. The inverse is obtained by replacing $\mathbf{P_0} \to -\mathbf{P_0}$ in the expression above. The free spin $\mathbf{j}_0$ is Hermitian, the components satisfy $SU(2)$ commutation relations and commute with P_0^μ. It represents the angular momentum of the system of particles in the rest frame of the non-interacting system assuming that the system was transformed to the rest frame with a non-interacting rotationless (canonical) Lorentz boost.

To construct the dynamical representation of the Poincaré group the first step is to construct simultaneous eigenstates of the commuting observables $M_0, \mathbf{P_0}, \mathbf{j}_0^2, \mathbf{j}_0 \cdot \hat{\mathbf{z}}$,

$$|(m_0, j_0)\mathbf{p}, \mu, d\rangle \tag{12}$$

for the non-interacting system, where d represents kinematically invariant degeneracy parameters. These eigenstates can be expressed as linear combinations of single particle states using Clebsch-Gordan coefficients of the Poincaré group, see Eq. (48) below. The next step is to add interactions, V, that commute with and are independent of $\mathbf{P_0}$ and commute with all three components of $\mathbf{j}_0$ to the non-interacting mass Casimir operator. This defines a dynamical mass operator

$$M = M_0 + V \tag{13}$$

where matrix elements of the interaction in the basis (12) have the form

$$\langle (m', j')\mathbf{p}', \mu', d'|V|(m, j)\mathbf{p}, \mu, d\rangle = \delta(\mathbf{p}' - \mathbf{p})\delta_{j'j}\delta_{\mu\mu'}\langle m'\, d'\|V^j\|m\, d\rangle. \tag{14}$$

In this expression d represents kinematically invariant degeneracy quantum numbers:

$$U_0(\Lambda, a)dU_0^\dagger(\Lambda, a) = d. \tag{15}$$

The degeneracy parameters depend on the model Hilbert space, but typically involve quantities like invariant masses and squares of angular momenta of subsystems. The kernel, $\langle m', d'\|V^j\|m, d\rangle$, of the reduced potential is the analog of a partial wave potential. Since V is not diagonal in the degeneracy observables they will no longer be invariant in the dynamical representation.

For V satisfying (14) the operators $M, \mathbf{P_0}, \mathbf{j}_0^2, \hat{\mathbf{z}} \cdot \mathbf{j}_0$ are mutually commuting self-adjoint operators. The dynamical mass operator M can be diagonalized in the basis (12) resulting in simultaneous eigenstates of $M, \mathbf{P_0}, \mathbf{j}_0^2, \hat{\mathbf{z}} \cdot \mathbf{j}_0$:

$$|(m, j)\mathbf{p}, \mu, \tilde{d}\rangle \tag{16}$$

where $\tilde{d}$ represent new dynamically invariant degeneracy parameters. These eigenstates transform like (2) with the single-particle mass replaced by the eigenvalues, m_I, of the dynamical mass operator M:

$$U(\Lambda, a)|(m_I, j)\mathbf{p}, \mu, \tilde{d}\rangle =$$

$$e^{-ip'\cdot a} \sum_{\nu=-j}^{j} |(m_I, j)\mathbf{p}', \nu, \tilde{d}\rangle \sqrt{\frac{E(\mathbf{p}')}{E(\mathbf{p})}}\, D^j_{\mu\nu}[R_w(\Lambda, p)]\,, \tag{17}$$

where

$$E(\mathbf{p}) = \sqrt{m_I^2 + \mathbf{p}^2}\,. \tag{18}$$

This construction is due to Bakamjian and Thomas [4]. It results in an explicit unitary representation of the Poincaré group. It has the property that the Lorentz boosts are interaction dependent. The interaction dependence appears in the dependence of the right side of (17) on the dynamical mass eigenvalues, so dynamical boosts can be computed once the mass operator (13) is diagonalized.

For the applications in this paper the construction discussed above will be used to model the strong interactions while the weak and electromagnetic interactions will be treated using the one-boson exchange approximation.

In the one-boson exchange approximation $U(\Lambda, a)$ factors into a tensor product of unitary representations of the Poincaré group for the strongly interacting baryons (B) and the leptons (L):

$$U(\Lambda, a) \approx U_B(\Lambda, a) \otimes U_L(\Lambda, a). \tag{19}$$

The coupling is through a current that couples to the exchanged boson. The current is a sum of a weak and strong current plus an interaction current

$$J^\mu(x) = J^\mu_B(x) + J^\mu_L(x) + J^\mu_I(x) \to J^\mu_B(x) + J^\mu_L(x), \tag{20}$$

where the interaction term includes the parts of the current that do not contribute to the one-boson exchange approximation and they will be ignored in what follows. The strong and

weak currents transform covariantly with respect to the baryonic, $U_B(\Lambda, a)$, and leptonic, $U_L(\Lambda, a)$, representations of the Poincaré group

$$U_A(\Lambda, a) J_A^\mu(x) U_A^\dagger(\Lambda, a) = (\Lambda^{-1})^\mu{}_\nu J_A^\nu(\Lambda x + a) \qquad \text{where} \qquad A = B, L. \tag{21}$$

Both $J_B^\mu(x)$ and $J_L^\mu(x)$ have cluster expansions as sums of one-body, two-body, $\cdots$ operators

$$J_A^\mu(x) = \sum_i J_{Ai}^\mu(x) + \frac{1}{2} \sum_{i \neq j} J_{Aij}^\mu(x) + \cdots \tag{22}$$

While the leptons can be approximately treated at tree level, where current covariance holds up to higher order corrections, the $2 \cdots N$-body parts of the baryon currents must be non-zero in order to satisfy the covariance and current conservation.

This can be seen from the commutation relations of the current operator with the dynamical generators of the Poincaré group. The cluster expansions for the current and rotationless boost generators, $\mathbf{K}$, have the form

$$J_B^\mu(0) = J_{B0}^\mu(0) + J_{BI}^\mu(0)\,, \qquad J_{B0}^\mu(0) = \sum_i J_{Bi}^\mu(0) \tag{23}$$

$$\mathbf{K} = \mathbf{K_0} + \mathbf{K_I}\,, \qquad \mathbf{K_0} = \sum_i \mathbf{K}_i \tag{24}$$

Since the current $J^\mu(0)$ transforms like P^μ under Lorentz transformations it has the same commutation relations with the boost generators as P^μ:

$$[K_0^i + K_I^i, J^i(0)] = i J^0(0)\,, \qquad [K_0^i + K_I^i, J^0(0)] = i J^i(0) \tag{25}$$

Cluster properties mean that (25) holds when the particles are asymptotically separated where $K_I^i \to K_0^i$ and $J_I^\mu(0) \to J_0^\mu(0)$. Canceling the one-body terms means that the interacting parts of the current $J_I^\mu(0)$ must satisfy

$$\begin{aligned} [K_0^i, J_I^i(0)] + [K_I^i, J_I^i(0)] - i J_I^0(0) &= [J_0^i(0), K_I^i], \\ [K_0^i, J_I^0(0)] + [K_I^i, J_I^0(0)] - i J_I^0(0) &= [J_0^0(0), K_I^i]. \end{aligned} \tag{26}$$

If the right side of either equation is non zero then the current must have many-body parts in order to satisfy current covariance. Similar conditions follow if the current is conserved.

In general, these many-body contributions to the current have to be supplemented by the many-body currents that arise from physical processes such as exchange of charged mesons. They are not uniquely determined from current covariance.

One way to ensure covariance is to use current matrix elements. Since current matrix elements transform covariantly, all current matrix elements can be generated from any independent set of matrix elements using covariance. Any model of the current can be used to compute an independent set of current matrix elements, while the remaining elements can be computed by requiring covariance. While this implicitly generates covariant current matrix elements, the current matrix elements will depend on the choice of independent current matrix elements. If the current operator used to calculate the independent matrix elements was exactly covariant the results would be independent of the choice of independent current matrix elements. In this work, since boosts are dynamical, impulse approximations in one frame are not equivalent to impulse approximations in another frame. Violations of current covariance at the operator level can be investigated by comparing calculations performed in different frames or based on different choices of independent current matrix elements.

A model of the strong interaction dynamics is defined by the interacting mass operator M. For the two nucleon-system it should have a discrete one-body eigenstate with the mass of a deuteron and should produce measured scattering observables. The scattering operator is a unitary operator that can be expressed in the form $S = e^{2i\delta}$ where δ is the phase shift operator. Since S is relativistically invariant, so are the phase shifts. Phenomenological non-relativistic interactions are constructed by (1) using data from experimentally measured cross sections (2) using correct relativistic kinematics to transform the laboratory cross sections to the center of momentum (3) adjusting potential parameters so the wave functions obtained by solving the Schrödinger equation give the correct phase shifts as a function of the center of momentum momenta, $\mathbf{k}$, of one of the particles. *An important observation is that even though the non-relativistic Schrödinger equation is used to extract the phase shifts, the data knows nothing about non-relativistic limits and the transformation of the data to the two-body rest frame is performed using the correct relativistic kinematics.* The phase shifts are experimental quantities that parameterize the relativistic scattering operator. The only place where the difference between the relativistic and non-relativistic treatment appears is whether the experimental phase shifts are identified as functions of energy, $\delta(E_{NR}) = \delta(E_R)$ for $E_{NR} = E_R$ or as functions of center of momentum momenta $\delta(\mathbf{k}^2_{NR}) = \delta(\mathbf{k}^2_R)$ for $|\mathbf{k}_{NR}| = |\mathbf{k}_R|$. This depends on how the potential is constructed; for the V18 potential used in this work the phase shifts are fit as functions $\mathbf{k}^2$. This means that if the dynamical mass operator is a function of the non-relativistic Schrödinger Hamiltonian, the wave functions

and phase shifts will be identical to the non-relativistic wave functions and phase shifts as a function of the relative momentum. These phase shifts are the "experimental'" phase shifts that define the physical (relativistic) scattering operator.

For

$$k^\mu := B^{-1}((\mathbf{p}_n + \mathbf{p}_p)/m_{np})^\mu{}_\nu \frac{1}{2}(p_p^\nu - p_n^\nu)$$

the free invariant mass (for equal mass nucleons) has the form

$$M_0 = 2\sqrt{m^2 + \mathbf{k}^2}. \tag{27}$$

The operator

$$M := 2\sqrt{m^2 + 2\mu\left(\frac{\mathbf{k}^2}{2\mu} + V_{NR}\right)}, \tag{28}$$

where μ is the reduced mass of the two-body system and V_{NR} a realistic non-relativistic two-body interaction, is a function of the non-relativistic Hamiltonian that becomes the two-body invariant mass in the limit that the interaction vanishes. A relativistic interaction is defined as the difference $V_R = M - M_0$:

$$V_R := 2\sqrt{m^2 + 2\mu\left(\frac{\mathbf{k}^2}{2\mu} + V_{NR}\right)} - 2\sqrt{m^2 + 2\mu\left(\frac{\mathbf{k}^2}{2\mu}\right)}. \tag{29}$$

There are a number of ways to diagonalize M, however the wave functions and phase shifts are identical to the ones obtained by solving the nonrelativistic Schrödinger equation. In this work V_R is calculated directly using the method outlined in [2], which involves solving a non-linear equation for V_R. In this work V_{NR} is taken as the Argonne V18 potential [3].

This model is formally applicable to calculations at energies below the threshold for pion production. The model can be extended to include pion degrees of freedom, but that extension is not considered in this work.

The general expression for the differential cross section is

$$d\sigma = \frac{(2\pi)^4}{v_r} \left|\langle \mathbf{p}_1, \mu_1, \cdots, \mathbf{p}_N, \mu_N \| T(E + i\epsilon) \| \mathbf{p}_B, \mu_B, \mathbf{p}_T, \mu_T \rangle\right|^2 \Pi_i d\mathbf{p}_i \, \delta^4(P_f - P_i)\,, \tag{30}$$

where v_r is the relative speed between the projectile and target, and P_f^μ and P_i^μ are the total final and initial four momentum of the system, and $T(z)$ is the transition operator with the total momentum conserving delta function removed:

$$\langle \mathbf{P}_t' \cdots' | T | \mathbf{P}_t \cdots \rangle = \delta(\mathbf{P}_t' - \mathbf{P}_t) \langle \cdots' \| T \| \cdots \rangle. \tag{31}$$

The differential cross section (30) can be expressed as a product of three invariant quantities

$$d\sigma = \frac{(2\pi)^4}{\sqrt{(p_B \cdot p_T)^2 - m_T^2 m_B^2}} \times$$

$$\Pi_i E_i(\mathbf{p}_i'^2) |\langle \mathbf{p}_1', \mu_1', \cdots \mathbf{p}_N', \mu_N' \| T(E_T + i\epsilon) \| \mathbf{p}_B, \mu_B, \mathbf{p}_T, \mu_T \rangle|^2 E_B(\mathbf{p}_B^2) E_T(\mathbf{p}_T^2) \times$$

$$\delta^4(P_f - P_i) \tag{32}$$

where the subscripts B and T stand for beam and target respectively. This form can be utilized in any frame. Specific cross sections are derived from (32) by integrating over the unmeasured kinematical quantities, including those fixed by the four-momentum conserving delta function.

In the one boson-exchange approximation, the transition matrix elements for a beam of electrons or neutrinos is

$$\langle \mathbf{p}_L', \mu_L', \mathbf{p}_1', \mu_1', \cdots \mathbf{p}_N' \mu_N' \| T(E_T + i\epsilon) \| \mathbf{p}_L, \mu_L, \mathbf{p}_T, \mu_T \rangle =$$

$$-(2\pi)^3 g^2 \langle \mathbf{p}_L', \mu_L' | J_L^\mu(0) | \mathbf{p}_L, \mu_L \rangle G_{\mu\nu}(p_l - p_l') \langle (\mathbf{p}_1', \mu_1' \cdots \mathbf{p}_N', \mu_N')^- | J_B^\nu(0) | \mathbf{p}_B', \mu_B' \rangle \,, \tag{33}$$

where

$$|(\mathbf{p}_1', \mu_1' \cdots \mathbf{p}_N', \mu_N')^- \rangle \tag{34}$$

can be a bound or scattering eigenstate,

$$G_{\mu\nu}(k) = i \int \langle 0 | T(V_\mu(x) V_\nu(0)) | 0 \rangle e^{ik\cdot x} d^4x \,, \tag{35}$$

where $V^\mu(x)$ is the field of the exchanged boson and g is the coupling constant of the interaction of the current with the exchanged boson

$$V_c = g \int d\mathbf{x} J^\mu(\mathbf{x}, t) V_\mu(\mathbf{x}, t) \tag{36}$$

for fixed t.

III. KINEMATICS AND MATRIX ELEMENTS

A. Kinematics and matrix elements for electron or neutrino elastic scattering off the deuteron

The four-momentum conservation for the $e + d \to e' + d'$ reaction in a general frame, where the total energy is E_t and the total momentum is denoted $\mathbf{P}_t$, reads

$$\begin{aligned} E_t &\equiv E_e + E_D = E'_e + E'_D \,, \\ \mathbf{P}_t &\equiv \mathbf{p}_e + \mathbf{p}_D = \mathbf{p}'_e + \mathbf{p}'_D \,, \end{aligned} \tag{37}$$

where $\mathbf{p}_e$ and $\mathbf{p}_D$ ($\mathbf{p}'_e$ and $\mathbf{p}'_D$) are the initial (final) electron and deuteron momenta, $E_e = \sqrt{m_e^2 + |\mathbf{p}_e|^2}$ and $E_D = \sqrt{m_D^2 + |\mathbf{p}_D|^2}$ ($E'_e = \sqrt{m_e^2 + |\mathbf{p}'_e|^2}$ and $E'_D = \sqrt{m_D^2 + |\mathbf{p}'_D|^2}$) are the corresponding total energies with m_e and m_D being the electron and deuteron masses. The system of equations (37) can be solved analytically to yield $|\mathbf{p}'_e|$ for a given electron scattering angle θ_e, which is the angle between $\mathbf{P}_t$ and $\mathbf{p}'_e$. For $\mathbf{P}_t = 0$ the electron scattering angle is taken between the initial $\mathbf{p}_e$ and final $\mathbf{p}'_e$ electron momentum. There is no restriction for θ_e: $0 \le \theta_e \le 180°$. We obtain

$$\begin{aligned} |\mathbf{p}'_e| = &\frac{E_t \sqrt{H + \left(2m_e |\mathbf{P}_t| \cos\theta_e\right)^2}}{2(E_t - \cos\theta_e |\mathbf{P}_t|)(E_t + \cos\theta_e |\mathbf{P}_t|)} \\ &+ \frac{|\mathbf{P}_t| \left({E_t}^2 - {m_D}^2 + {m_e}^2 - |\mathbf{P}_t|^2\right) \cos\theta_e}{2(E_t - \cos\theta_e |\mathbf{P}_t|)(E_t + \cos\theta_e |\mathbf{P}_t|)} \end{aligned} \tag{38}$$

with $H \equiv E_t^4 + \left(m_D^2 - m_e^2 + |\mathbf{P}_t|^2\right)^2 - 2E_t^2(m_D^2 + m_e^2 + |\mathbf{P}_t|^2)$. In the laboratory frame, where $\mathbf{P}_t = \mathbf{p}_e$, $E_t = m_D + E_e$, and neglecting the electron mass equation (38) reduces to the simple result well known from the Compton scattering:

$$|\mathbf{p}'_e| = \frac{m_D |\mathbf{p}_e|}{m_D + |\mathbf{p}_e| \left(1 - \cos\theta_e\right)} \,, \tag{39}$$

which is sufficient for all our calculations performed in this frame.

The transition matrix elements for this reaction in the one-photon-exchange approximation are given as contractions of the electron

$$\langle \mathbf{p}'_e, \mu'_e | J_e^\nu(0) | \mathbf{p}_e, \mu_e \rangle$$

and nuclear (here deuteron "D")

$$\langle \mathbf{p}'_D, \mu'_D, D | J^\mu_{nuc,EM}(0) | \mathbf{p}_D, \mu_D, D \rangle$$

matrix elements:

$$\langle \mathbf{p}'_D, \mu'_D, D, \mathbf{p}'_e, \mu'_e \| T_{eD} \| \mathbf{p}_D, \mu_D, D, \mathbf{p}_e, \mu_e \rangle =$$
$$-e^2 (2\pi)^3 \langle \mathbf{p}'_D, \mu'_D, D | J^\mu_{nuc,EM}(0) | \mathbf{p}_D, \mu_D, D \rangle \, \frac{g_{\mu\nu}}{(p'_e - p_e)^2 + i\epsilon} \, \langle \mathbf{p}'_e, \mu'_e | J^\nu_e(0) | \mathbf{p}_e, \mu_e \rangle \,, \quad (40)$$

with $e^2 = 4\pi\alpha$, where $\alpha \approx \frac{1}{137}$ is the fine structure constant. The differential cross section in terms of (40) becomes

$$\mathrm{d}\sigma = \frac{(2\pi)^4 E_D E_e}{\sqrt{(p_D \cdot p_e)^2 - m_D^2 m_e^2}} |\langle \mathbf{p}'_D, \mu'_D, D, \mathbf{p}'_e, \mu'_e \| T_{eD} \| \mathbf{p}_D, \mu_D, D, \mathbf{p}_e, \mu_e \rangle|^2$$
$$\times E'_D E'_e \delta^4(p_D + p_e - p'_D - p'_e) \frac{\mathrm{d}\mathbf{p}'_D}{E'_D} \frac{\mathrm{d}\mathbf{p}'_e}{E'_e} \quad (41)$$

and is a product of the following three invariant factors

$$\frac{(2\pi)^4}{\sqrt{(p_D \cdot p_e)^2 - m_D^2 m_e^2}} \,, \quad (42)$$

$$E'_D E'_e \, |\langle \mathbf{p}'_D, \mu'_D, D, \mathbf{p}'_e, \mu'_e \| T_{eD} \| \mathbf{p}_D, \mu_D, D, \mathbf{p}_e, \mu_e \rangle|^2 \, E_D E_e \,, \quad (43)$$

and

$$\delta^4(p_D + p_e - p'_D - p'_e) \frac{\mathrm{d}\mathbf{p}'_D}{E'_D} \frac{\mathrm{d}\mathbf{p}'_e}{E'_e} \,. \quad (44)$$

(Note the momentum eigenstates have a delta function normalization $\langle \mathbf{p}' | \mathbf{p} \rangle = \delta(\mathbf{p}' - \mathbf{p})$.)

In terms of Dirac spinors

$$u(\mathbf{p}, \mu) = \sqrt{\frac{\sqrt{m^2 + |\mathbf{p}|^2} + m}{2m}} \begin{pmatrix} \chi_\mu \\ \frac{\mathbf{p}\cdot\boldsymbol{\sigma}}{\sqrt{m^2+|\mathbf{p}|^2}+m} \chi_\mu \end{pmatrix}$$

with the Bjorken-Drell [5] conventions and normalization $\bar{u}(\mathbf{p}, \mu) u(\mathbf{p}, \mu) = 1$, the electron current matrix elements can be expressed as

$$\langle \mathbf{p}'_e, \mu'_e | J^\nu_e(0) | \mathbf{p}_e, \mu_e \rangle = \frac{1}{(2\pi)^3} \sqrt{\frac{m_e^2}{E_e E'_e}} \bar{u}_e(\mathbf{p}'_e, \mu'_e) \gamma^\nu u_e(\mathbf{p}_e, \mu_e) \quad (45)$$
$$\equiv \frac{1}{(2\pi)^3} \sqrt{\frac{1}{4 E_e E'_e}} \, L^\nu_e \left(\mathbf{p}'_e, \mu'_e, \mathbf{p}_e, \mu_e \right) \,, \quad (46)$$

where in (46) the mass factor $\frac{1}{2m_e}$ is extracted from $\bar{u}_e(\mathbf{p}'_e, \mu'_e) \gamma^\nu u_e(\mathbf{p}_e, \mu_e)$. The latter form can be used also in the reactions with (approximately massless) neutrinos.

In order to calculate the deuteron current matrix element,

$$\langle \mathbf{p}'_D, \mu'_D, D | J^\mu_{nuc,EM}(0) | \mathbf{p}_D, \mu_D, D \rangle \equiv \frac{1}{(2\pi)^3} \, N^\mu_{eD} \left(\mathbf{p}'_D, \mu'_D, \mathbf{p}_D, \mu_D \right) \,, \quad (47)$$

we have to recall our choice of noninteracting irreducible states and the resulting Poincaré Clebsch-Gordan coefficients [6–8]

$$\begin{aligned}
&\langle \mathbf{p}_1, \mu_1, \mathbf{p}_2, \mu_2 | (j,k) \mathbf{p}, \mu; l, s \rangle \\
&= \sum_{\mu_l \mu_s \mu_1' \mu_2'} \delta(\mathbf{p} - \mathbf{p}_1 - \mathbf{p}_2) \frac{\delta(k - k(\mathbf{p}_1, \mathbf{p}_2))}{k^2} \mathcal{N}^{-1}(\mathbf{p}_1, \mathbf{p}_2)\, Y_{l\mu_l}(\hat{\mathbf{k}}(\mathbf{p}_1, \mathbf{p}_2)) \\
&\qquad \times D^{1/2}_{\mu_1 \mu_1'}[R_w(B(\mathbf{p}/m_{120}), \mathbf{k}_1)]\, D^{1/2}_{\mu_2 \mu_2'}[R_w(B(\mathbf{p}/m_{120}), \mathbf{k}_2)] \\
&\qquad \times (l, \mu_l, s, \mu_s | j, \mu)(1/2, \mu_1', 1/2, \mu_2' | s, \mu_s) \\
&= \int \mathrm{d}\hat{\mathbf{k}} \sum_{\mu_l \mu_s \mu_1' \mu_2'} \delta(\mathbf{p}_1 - \mathbf{p}_1(\mathbf{p}, \mathbf{k})) \delta(\mathbf{p}_2 - \mathbf{p}_2(\mathbf{p}, \mathbf{k}))\, \mathcal{N}(\mathbf{p}_1, \mathbf{p}_2)\, Y_{l\mu_l}(\hat{\mathbf{k}}) \\
&\qquad \times D^{1/2}_{\mu_1 \mu_1'}[R_w(B(\mathbf{p}/m_{120}), \mathbf{k}_1)]\, D^{1/2}_{\mu_2 \mu_2'}[R_w(B(\mathbf{p}/m_{120}), \mathbf{k}_2)] \\
&\qquad \times (l, \mu_l, s, \mu_s | j, \mu)(1/2, \mu_1', 1/2, \mu_2' | s, \mu_s)\,. \qquad (48)
\end{aligned}$$

In these expressions $m_{120} = \sqrt{m^2 + \mathbf{p}_1^2} + \sqrt{m^2 + \mathbf{p}_2^2}$ is replaced by $\sqrt{\mathbf{k}^2}$, where m is the nucleon mass, $(j_1, \mu_1, j_2, \mu_2 | j_3, \mu_3)$ are $SU(2)$ Clebsch-Gordan coefficients, $D^{1/2}_{\mu'\mu}[R]$ is the Wigner D-matrix for spin $1/2$. The $\mathbf{k}_i$ are the three-vector components of $k_i = B^{-1}(\mathbf{p}/m_{120})p_i$. Arguments of the latter, $R_w(B(\mathbf{p}/m_{120}), \mathbf{k}_i)$, are Wigner rotations resulting from a product of three rotationless Lorentz transformations

$$R_w(B(\mathbf{p}/m_{120}), \mathbf{k}_i) = B^{-1}(\mathbf{p}_i/m) B(\mathbf{p}/m_{120}) B(\mathbf{k}_i/m)\,, \qquad (49)$$

where $B(\mathbf{k}_i/m)$ takes a particle of mass m at rest to momentum $\mathbf{k}_i$, $B(\mathbf{p}/m_{120})$ takes a system of two particles with the same mass, m, and momenta $\mathbf{k} = \mathbf{k}_1$ and $-\mathbf{k} = \mathbf{k}_2$, respectively, to the total two-particle momentum $\mathbf{p}$, by which the momentum $\mathbf{k}_i$ is changed to $\mathbf{p}_i$. Finally, $B^{-1}(\mathbf{p}_i/m)$ brings the particle with the momentum $\mathbf{p}_i$ to its rest frame. Here $B(\mathbf{p}/m)^\mu{}_\nu$ is the rotationless Lorentz transformation that takes $(m, 0, 0, 0)$ to $(E(\mathbf{p}), \mathbf{p})$ (see Eqs. (6)–(7)). The normalization coefficients

$$\mathcal{N}^{-2}(\mathbf{p}_1, \mathbf{p}_2) = \frac{E(\mathbf{k}) E(\mathbf{k}) (E(\mathbf{p}_1) + E(\mathbf{p}_2))}{E(\mathbf{p}_1) E(\mathbf{p}_2) (E(\mathbf{k}) + E(\mathbf{k}))}\,, \qquad (50)$$

ensure unitarity of the Clebsch Gordon coefficients for basis states with delta function normalizations.

The Bjorken and Drell spinors are also representations of the canonical boost; the spins undergo the same Wigner rotations under Lorentz transformations:

$$\sum_b S(\Lambda)_{ab} u_b(\mathbf{p}, \mu) = \sum_\nu u_a(\Lambda p, \nu) D^{1/2}_{\nu\mu}[R_w(\Lambda, \mathbf{p})], \qquad (51)$$

where $S(\Lambda)$ is the 4×4 Dirac spinor representation of the Lorentz group. The relativistic counterpart of the center of mass relative momentum is obtained by replacing a Galilean boost applied to half of the relative momentum to the zero momentum frame by a canonical boost to the zero momentum frame of the non-interacting two body system:

$$\begin{aligned}\mathbf{k} \equiv \mathbf{k}(\mathbf{p}_1, \mathbf{p}_2) = \mathbf{B}^{-1}(\mathbf{p}/m_{120}) \left(\frac{1}{2} (p_1 - p_2) \right) = \\ = \frac{1}{2} \left(\mathbf{p}_1 - \mathbf{p}_2 - \frac{(E(\mathbf{p}_1) - E(\mathbf{p}_2)) (\mathbf{p}_1 + \mathbf{p}_2)}{E(\mathbf{p}_1) + E(\mathbf{p}_2) + \sqrt{(E(\mathbf{p}_1) + E(\mathbf{p}_2))^2 - (\mathbf{p}_1 + \mathbf{p}_2)^2}} \right) . \end{aligned} \tag{52}$$

Conversely, the individual momenta $\mathbf{p}_1$ and $\mathbf{p}_2$ can be calculated from $\mathbf{p}$ and $\mathbf{k}$ in the following way:

$$\begin{aligned}\mathbf{p}_1 \equiv \mathbf{p}_1(\mathbf{p}, \mathbf{k}) = \mathbf{k} + \frac{1}{2}\mathbf{p} + \frac{(\mathbf{p} \cdot \mathbf{k})\, \mathbf{p}}{2E(\mathbf{k})(E_{12}(\mathbf{p}, \mathbf{k}) + 2E(\mathbf{k}))} , \\ \mathbf{p}_2 \equiv \mathbf{p}_2(\mathbf{p}, \mathbf{k}) = -\mathbf{k} + \frac{1}{2}\mathbf{p} - \frac{(\mathbf{p} \cdot \mathbf{k})\, \mathbf{p}}{2E(\mathbf{k})(E_{12}(\mathbf{p}, \mathbf{k}) + 2E(\mathbf{k}))} \end{aligned} \tag{53}$$

where $E_{12}(\mathbf{p}, \mathbf{k}) = \sqrt{(2E(\mathbf{k}))^2 + \mathbf{p}^2}$. Note that $\mathbf{k}$ does not transform like the space component of a four vector; instead it undergoes Wigner rotation $\mathbf{k} \to \mathbf{k}' = R_w(\Lambda, \mathbf{p})\, \mathbf{k}$ for $p' = \Lambda p$. This means $k^2 := \mathbf{k}^2$ is kinematically invariant. The quantum numbers l and s are also kinematically invariant degeneracy parameters that distinguish representations with the same mass (k) and spin (j). For a two-nucleon system they have the same spectrum as the orbital and spin angular momentum operators in a partial wave representation of the nonrelativistic basis [6–8].

This information is used to express the deuteron state in terms of the "relativistic partial waves":

$$\langle (j,k)\mathbf{P}, \mu; l, s; t, \tau | \mathbf{p}_D, \mu_D, D \rangle \; = \; \delta \left(\mathbf{P} - \mathbf{p}_D \right) \, \delta_{j1} \, \delta_{\mu \mu_D} \, \delta_{s1} \, \delta_{t0} \, \delta_{\tau 0} \, \phi_{D,l}(k) \, , \tag{54}$$

where $\phi_{D,l}(k)$ are the s ($l = 0$) and d ($l = 2$) components of the deuteron wave function. Note that we added here isospin quantum numbers: t is the total two-nucleon isospin and τ

is the value of its z-component. The formal structure of the current matrix element (47) is

$$\begin{aligned}
&\langle \mathbf{p}'_D, \mu'_D, D | J^{\mu}_{nuc,EM}(0) | \mathbf{p}_D, \mu_D, D \rangle \\
&= \int \mathrm{d}\mathbf{p}' \sum_{l'=0,2} \int \mathrm{d}k' k'^2 \int \mathrm{d}\mathbf{p}'_1 \sum_{\mu'_1,\tau'_1} \int \mathrm{d}\mathbf{p}'_2 \sum_{\mu'_2,\tau'_2} \\
&\int \mathrm{d}\mathbf{p}_1 \sum_{\mu_1,\tau_1} \int \mathrm{d}\mathbf{p}_2 \sum_{\mu_2,\tau_2} \int \mathrm{d}\mathbf{p} \sum_{l=0,2} \int \mathrm{d}k k^2 \\
&\langle \mathbf{p}'_D, \mu'_D, D | (1,k')\mathbf{p}', \mu'; l', 1; 0, 0 \rangle \\
&\langle (1,k')\mathbf{p}', \mu'; l', 1; 0, 0 | \mathbf{p}'_1, \mu'_1, \tau'_1, \mathbf{p}'_2, \mu'_2, \tau'_2 \rangle \\
&\langle \mathbf{p}'_1, \mu'_1, \tau'_1, \mathbf{p}'_2, \mu'_2, \tau'_2 | J^{\mu}_{nuc,EM}(0) | \mathbf{p}_1, \mu_1, \tau_1, \mathbf{p}_2, \mu_2, \tau_2 \rangle \\
&\langle \mathbf{p}_1, \mu_1, \tau_1, \mathbf{p}_2, \mu_2, \tau_2 | (1,k)\mathbf{p}, \mu; l, 1; 0, 0 \rangle \\
&\langle (1,k)\mathbf{p}, \mu; l, 1; 0, 0 | \mathbf{p}_D, \mu_D, D \rangle \,, \qquad (55)
\end{aligned}$$

where τ_i and τ'_i denote the isospin projections in the single-nucleon states. Matrix elements (55) comprise contributions from single-nucleon current and two-nucleon current operators:

$$\begin{aligned}
&\langle \mathbf{p}'_1, \mu'_1, \tau'_1, \mathbf{p}'_2, \mu'_2, \tau'_2 | J^{\mu}_{nuc,EM}(0) | \mathbf{p}_1, \mu_1, \tau_1, \mathbf{p}_2, \mu_2, \tau_2 \rangle \\
&= \delta(\mathbf{p}'_1 - \mathbf{p}_1)\, \delta_{\mu'_1\mu_1}\, \delta_{\tau'_1\tau_1}\, \langle \mathbf{p}'_2, \mu'_2, \tau'_2 | J^{\mu}_{2,EM}(0) | \mathbf{p}_2, \mu_2, \tau_2 \rangle \\
&+ \delta(\mathbf{p}'_2 - \mathbf{p}_2)\, \delta_{\mu'_2\mu_2}\, \delta_{\tau'_2\tau_2}\, \langle \mathbf{p}'_1, \mu'_1, \tau'_1 | J^{\mu}_{1,EM}(0) | \mathbf{p}_1, \mu_1, \tau_1 \rangle \\
&+ \langle \mathbf{p}'_1, \mu'_1, \tau'_1, \mathbf{p}'_2, \mu'_2, \tau'_2 | J^{\mu}_{\{1,2\},EM}(0) | \mathbf{p}_1, \mu_1, \tau_1, \mathbf{p}_2, \mu_2, \tau_2 \rangle \,. \qquad (56)
\end{aligned}$$

In this paper we neglect two-nucleon current contribution and discuss consequences of such an approximation in Sec. IV. Since the deuteron state and the two-nucleon scattering states are antisymmetric with respect to the exchange of nucleons 1 and 2, it is sufficient to consider the contribution from $J^{\mu}_{1,EM}(0)$ and multiply the result by 2 in order to account for the $J^{\mu}_{2,EM}(0)$ part. The electromagnetic single-nucleon current operator has a well known form

$$\begin{aligned}
&\langle \mathbf{p}', \mu', \tau' | J^{\mu}_{k,EM}(0) | \mathbf{p}, \mu, \tau \rangle = \delta_{\tau'\tau} \frac{1}{(2\pi)^3} \sqrt{\frac{m^2}{E(\mathbf{p}')E(\mathbf{p})}} \\
&\times \bar{u}(\mathbf{p}', \mu') \left(\gamma^{\mu} F_{1,\tau}(Q^2) + i \frac{(p'_{\alpha} - p_{\alpha}) \sigma^{\mu\alpha}}{2m} F_{2,\tau}(Q^2) \right) u(\mathbf{p}, \mu) \,, \qquad (57)
\end{aligned}$$

where $F_{1,\tau}$ and $F_{2,\tau}$ are the Dirac and Pauli proton (for $\tau = 1/2$) or neutron (for $\tau = -1/2$) electromagnetic form factors, which depend on the square of the four momentum transferred to the nucleon, $Q^2 \equiv -(p'-p)_{\alpha}(p'-p)^{\alpha}$. (Note that we neglect the small difference between

the proton and neutron mass, so m is the average nucleon mass.) For selected observables we compare, in Sec. IV, results based on a few recent models of the electromagnetic nucleon form factors [9–12].

Formulas for nuclear current matrix elements not only in elastic reactions but also in deuteron breakup processes follow from Eq. (56), the Poincaré Clebsch-Gordan coefficients (48) and the deuteron (54) or the two-nucleon scattering wave function. More details can be found in the appendix.

We now return to Eq. (41) and calculate the cross section, first for elastic electron-deuteron scattering in the laboratory frame. We define the energy transfer $\omega \equiv E_e - E'_e$ and set the three-momentum transfer $\mathbf{q} \equiv \mathbf{p}_e - \mathbf{p}'_e$ to be parallel to the z-axis. In this frame thus

$$\begin{aligned}
p_{ex} &= |\mathbf{p}_e||\mathbf{p}'_e| \sin\theta_e/|\mathbf{q}| \,, \\
p_{ey} &= 0 \,, \\
p_{ez} &= |\mathbf{p}_e| \left(|\mathbf{p}_e| - |\mathbf{p}'_e| \cos\theta_e \right)/|\mathbf{q}| \,, \\
p'_{ex} &= p_{ex} \,, \\
p'_{ey} &= 0 \,, \\
p'_{ez} &= |\mathbf{p}'_e| \left(-|\mathbf{p}'_e| + |\mathbf{p}_e| \cos\theta_e \right)/|\mathbf{q}| \,, \\
\mathbf{p}_D &= 0 \,, \\
\mathbf{p}'_D &= \mathbf{q} \,.
\end{aligned} \tag{58}$$

Further steps are standard. The electron mass m_e is neglected, nuclear current conservation

$$\omega \, N^0_{eD} = \mathbf{q} \cdot \mathbf{N}_{eD} \tag{59}$$

is used to express $N_{eD,z} \equiv N^3_{eD}$ in terms of N^0_{eD},

$$N_{eD,z} = \frac{\omega}{|\mathbf{q}|} \, N^0_{eD} \,, \tag{60}$$

some factors are used to build the Mott cross section

$$\sigma_{Mott} = \frac{\alpha^2 \cos^2\theta_e}{4|\mathbf{p}_e|^2 \, \sin^4 \frac{\theta_e}{2}} \,, \tag{61}$$

the phase space factor ρ_{elas} yields

$$\rho_{elas} \equiv \int \mathrm{d}\mathbf{p}'_e \int \mathrm{d}\mathbf{p}'_D \, \delta^4(p_D + p_e - p'_D - p'_e) = \int \mathrm{d}\hat{\mathbf{p}}'_e \, \frac{E'_D |\mathbf{p}'_e|^3}{m_D |\mathbf{p}_e|} \tag{62}$$

and finally, the contraction of the electron and nuclear matrix elements

$$\left(L_{e,\alpha}\left(\mathbf{p}'_e,\mu'_e,\mathbf{p}_e,\mu_e\right)\right)^*\; L_{e,\beta}\left(\mathbf{p}'_e,\mu'_e,\mathbf{p}_e,\mu_e\right)\; \left(N^{\alpha}_{eD}\right)^*\, N^{\beta}_{eD} \tag{63}$$

is evaluated [13]. The latter can be done under various assumptions. In the simplest case the initial electron is unpolarized and polarization of the final electron is not measured. Then we average over μ_e and sum over μ'_e. Alternatively, the initial electron can have a definite helicity $h = 1$ or $h = -1$, while we still sum over μ'_e. In such a case the two-component spinor χ_{μ_e} in (45) and (46) is chosen to fulfill

$$\mathbf{p}_e \cdot \boldsymbol{\sigma}\chi_{\mu_e} = h|\mathbf{p}_e|\chi_{\mu_e}\,.$$

The deuteron spin quantum numbers (not shown here for the sake of brevity) can be still chosen at will. However, the unpolarized laboratory frame differential cross section is studied most often (see for example [14–16]). It contains the structure functions $A(Q^2)$ and $B(Q^2)$, which experimentally are obtained through a Rosenbluth separation [17]:

$$\frac{\mathrm{d}\sigma}{\mathrm{d}\hat{\mathbf{p}}'_e}(Q^2,\theta_e) = \sigma_{Mott}\,\left(A(Q^2) + B(Q^2)\tan^2\left(\frac{\theta_e}{2}\right)\right)\,\frac{|\mathbf{p}'_e|}{|\mathbf{p}_e|}\,, \tag{64}$$

where Q^2 is now the square of the four momentum transferred to the deuteron. The frequently considered polarization observable is the deuteron tensor analyzing power $T_{20}(Q^2,\theta_e)$ at θ_e= 70° [18], which is obtained from the cross sections for the unpolarized initial and final electrons but for the initial deuterons with canonical spin polarizations μ_D= 1 and μ_D= 0:

$$T_{20}(Q^2,\theta_e) = \frac{\sqrt{2}\,\left(\frac{\mathrm{d}\sigma}{\mathrm{d}\hat{\mathbf{p}}'_e}(Q^2,\theta_e;\mu_D=1) - \frac{\mathrm{d}\sigma}{\mathrm{d}\hat{\mathbf{p}}'_e}(Q^2,\theta_e;\mu_D=0)\right)}{\frac{\mathrm{d}\sigma}{\mathrm{d}\hat{\mathbf{p}}'_e}(Q^2,\theta_e)}\,. \tag{65}$$

The kinematics of the neutral-current (NC) driven $\nu + d \to \nu' + d'$ reaction is the same as in elastic electron-deuteron scattering, provided the electron mass is neglected. We will describe this reaction using the approximate "current-current" theory, which allows us to employ the same formalism as before for electron scattering.

The transition matrix element for this process is

$$\begin{aligned}&\langle \mathbf{p}'_D,\mu'_D,D,\mathbf{p}'_\nu,\mu'_\nu\|T_{\mathrm{WNC}}\|\mathbf{p}_D,\mu_D,D,\mathbf{p}_\nu,\mu_\nu\rangle = \\ -\frac{G_F}{\sqrt{2}}(2\pi)^3&\langle \mathbf{p}'_D,\mu'_D,D|J^{\alpha}_{\mathrm{WNC}}(0)|\Phi_D|\mathbf{p}_D,\mu_D,D\rangle g_{\alpha\beta}\langle \mathbf{p}'_\nu,\mu'_\nu|J^{\beta}_{\nu}(0)|\mathbf{p}_\nu,\mu_\nu\rangle\,,\end{aligned} \tag{66}$$

where G_F is the Fermi constant. The neutrino current matrix element is written as

$$\langle \mathbf{p}'_\nu, \mu'_\nu | J^\beta_\nu(0) | \mathbf{p}_\nu, \mu_\beta \rangle \equiv \frac{1}{(2\pi)^3} \frac{1}{\sqrt{4|\mathbf{p}_\nu||\mathbf{p}'_\nu|}} \, L^\beta_\nu \left(\mathbf{p}'_\nu, \mu'_\nu, \mathbf{p}_\nu, \mu_\nu \right) \, , \tag{67}$$

with

$$L^\beta_\nu \left(\mathbf{p}'_\nu, \mu'_\nu, \mathbf{p}_\nu, \mu_\nu \right) = \bar{u}_\nu(\mathbf{p}'_\nu, \mu'_\nu) \gamma^\beta \left(1 - \gamma_5 \right) u_\nu(\mathbf{p}_\nu, \mu_\nu) \tag{68}$$

and the Dirac spinors for massless neutrinos defined as

$$u_\nu(\mathbf{p}_\nu, \mu_\nu) = \sqrt{|\mathbf{p}_\nu|} \begin{pmatrix} \chi_{\mu_\nu} \\ \frac{\mathbf{p}_\nu \cdot \boldsymbol{\sigma}}{|\mathbf{p}_\nu|} \chi_{\mu_\nu} \end{pmatrix} \, . \tag{69}$$

Also for weak reactions we include in the nuclear matrix elements

$$\langle \mathbf{p}'_D, \mu'_D, D | J^\alpha_{\rm WNC}(0) | \mathbf{p}_D, \mu_D, D \rangle \, \equiv \, \frac{1}{(2\pi)^3} \, N^\alpha_{\nu D} \left(\mathbf{p}'_D, \mu'_D, \mathbf{p}_D, \mu_D \right) \, ,$$

only the single-nucleon contributions:

$$\begin{aligned} & \langle \mathbf{p}', \mu', \tau' | \, J^\mu_{k,\rm WNC}(0) \, | \mathbf{p}, \mu, \tau \rangle \\ = \, & \delta_{\tau'\tau} \, \bar{u}(\mathbf{p}', \mu') \left(F^N_{1,\tau}(Q^2) \gamma^\mu + \frac{i}{2m} \sigma^{\mu\nu} q_\nu F^N_{2,\tau}(Q^2) \right. \\ & \left. + F^N_{A,\tau}(Q^2) \gamma^\mu \gamma_5 + \frac{q^\mu}{m} \gamma_5 F^N_{P,\tau}(Q^2) \right) u(\mathbf{p}, \mu) \, , \end{aligned} \tag{70}$$

where $q^\mu = p'^\mu - p^\mu$ and the weak neutral-current nucleon form factors $F^N_{i,\tau}$ depend on the nucleon isospin. For these quantities we use the parametrizations from Refs. [9, 12]. The part with $F^N_{P,\tau}$ gives no contribution in Eq. (70) in the case of massless neutrinos but we keep it, since the single nucleon charged current has the same functional form, with a different isospin dependence.

The steps leading to the cross section are standard. We denote in particular

$$\widetilde{L}_{\alpha\beta} \left(\mathbf{p}'_\nu, \mathbf{p}_\nu \right) \equiv \sum_{\mu_\nu \mu'_\nu} \left(L_{\nu,\alpha} \left(\mathbf{p}'_\nu, \mu'_\nu, \mathbf{p}_\nu, \mu_\nu \right) \right)^* \, L_{\nu,\beta} \left(\mathbf{p}'_\nu, \mu'_\nu, \mathbf{p}_\nu, \mu_\nu \right) \tag{71}$$

and obtain an intermediate result for the unpolarized case

$$\begin{aligned} {\rm d}\sigma = & \frac{G_F^2}{32\pi^2} \frac{E_D}{|\mathbf{p}'_\nu|} \frac{1}{|p_D \cdot p_\nu|} \widetilde{L}_{\alpha\beta} \left(\mathbf{p}'_\nu, \mathbf{p}_\nu \right) \\ & \times \frac{1}{3} \sum_{\mu'_D \mu_D} \left(N^\alpha \left(\mathbf{p}'_D, \mu'_D, \mathbf{p}_D, \mu_D \right) \right)^* N^\beta \left(\mathbf{p}'_D, \mu'_D, \mathbf{p}_D, \mu_D \right) \\ & \times \delta^4(p_D + p_\nu - p'_D - p'_\nu) {\rm d}\mathbf{p}'_D {\rm d}\mathbf{p}'_\nu \, . \end{aligned} \tag{72}$$

This result can be used together with the laboratory frame kinematics (58) or to calculate the differential cross section in the total momentum zero frame ("c.m."), where

$$\begin{aligned}
p_{\nu x} &= w\cos\left(\theta_{c.m.}/2\right)\,, \\
p_{\nu y} &= 0\,, \\
p_{\nu z} &= w\sin\left(\theta_{c.m.}/2\right)\,, \\
p'_{\nu x} &= p_{\nu x}\,, \\
p'_{\nu y} &= 0\,, \\
p'_{\nu z} &= -p_{\nu z}\,, \\
\mathbf{p}_D &= -\mathbf{p}_\nu\,, \\
\mathbf{p}'_D &= -\mathbf{p}'_\nu
\end{aligned} \tag{73}$$

and $w = |\mathbf{p}_D| = |\mathbf{p}_\nu| = |\mathbf{p}'_D| = |\mathbf{p}'_\nu|$. In the "c.m." frame the differential cross section can be written as

$$\left.\frac{\mathrm{d}\sigma}{\mathrm{d}\hat{\mathbf{p}}'_\nu}\right|_{c.m.} = \frac{G_F^2}{32\pi^2}\frac{E_D^2(\mathbf{p}_D)}{s}\widetilde{L}_{\alpha\beta}\,\frac{1}{3}\sum_{\mu'_D\mu_D} N^{*\alpha}_{\nu D}N^{\beta}_{\nu D}\,, \tag{74}$$

with $s \equiv (p_\nu + p_D)^2 = m_D\left(m_D + 2|\mathbf{p}_{\nu,lab}|\right)$ and $w = \frac{s-m_D^2}{2\sqrt{s}}$. The corresponding expression in the laboratory frame reads

$$\left.\frac{\mathrm{d}\sigma}{\mathrm{d}\hat{\mathbf{p}}'_\nu}\right|_{lab} = \frac{G_F^2}{32\pi^2}\frac{|\mathbf{p}'_\nu|^2}{|\mathbf{p}_\nu|^2}\frac{E'_D}{m_D}\widetilde{L}_{\alpha\beta}\,\frac{1}{3}\sum_{\mu'_D\mu_D} N^{*\alpha}_{\nu D}N^{\beta}_{\nu D}\,. \tag{75}$$

In both frames we can use the analytical result for $\widetilde{L}_{\alpha\beta}$,

$$\widetilde{L}_{\alpha\beta} = 8\left(p_{\nu\alpha}p'_{\nu\beta} + p'_{\nu\alpha}p_{\nu\beta} - (p_\nu\cdot p'_\nu)g_{\alpha\beta} + i\epsilon_{\alpha\beta\rho\sigma}p_\nu{}^\rho p'_\nu{}^\sigma\right)\,, \tag{76}$$

to evaluate the contraction $\widetilde{L}_{\alpha\beta}\,\frac{1}{3}\sum_{\mu'_D\mu_D} N^{*\alpha}_{\nu D}N^{\beta}_{\nu D}$. Here $\epsilon_{\alpha\beta\rho\sigma}$ is the totally antisymmetric Levi-Civita symbol with $\epsilon_{0123} = 1$. Note that for the choices of kinematics (58) or (73) some of the terms in this sum are identically zero.

Finally, we evaluate the total elastic cross section σ^{el}

$$\sigma^{el} = \int \mathrm{d}\hat{\mathbf{p}}'_\nu\frac{\mathrm{d}\sigma}{\mathrm{d}\mathbf{p}'_\nu} \equiv \int_0^{2\pi}\mathrm{d}\phi'\int_0^{\pi}\mathrm{d}\theta'\sin\theta'\,\frac{\mathrm{d}\sigma}{\mathrm{d}\mathbf{p}'_\nu} = 2\pi\int_0^{\pi}\mathrm{d}\theta'\sin\theta'\,\left.\frac{\mathrm{d}\sigma}{\mathrm{d}\mathbf{p}'_\nu}\right|_{\phi'=0}\,, \tag{77}$$

where θ' and ϕ' are the polar and azimuthal angles corresponding to $\mathbf{p}'_\nu$. A comparison of results for σ^{el} obtained in the "c.m." and laboratory frames can be used to test the relativistic character of the calculations. While in principle they should be the same, current covariance

requires two-body currents which are not treated in these calculations. The difference in the cross section calculations in different frames provides a measure of the impact of the two-body currents.

In our nonrelativistic calculations we use nonrelativistic kinematics and a nonrelativistic form of the current operator, which can be derived from Eq. (70). In addition to the strict nonrelativistic limit one can retain $(p/m)^2$ corrections stemming from a p/m expansion of the relativistic current operator. The density part is then

$$\begin{aligned}
&\langle \mathbf{p}', \mu', \tau' |\, J^0_{k,\mathrm{NR-WNC}}(0)\, | \mathbf{p}, \mu, \tau \rangle \\
&\qquad = \delta_{\tau'\tau} \chi^\dagger_{\mu'} \Bigg[F^N_{1,\tau} - (F^N_{1,\tau} + 2F^N_{2,\tau}) \frac{(\mathbf{p}' - \mathbf{p})^2}{8m^2} + (F^N_{1,\tau} + 2F^N_{2,\tau}) i \frac{(\mathbf{p}' \times \mathbf{p}) \cdot \boldsymbol{\sigma}}{4m^2} \\
&\qquad\qquad + F^N_{A,\tau} \frac{\boldsymbol{\sigma} \cdot (\mathbf{p} + \mathbf{p}')}{2m} + F^N_{P,\tau} \frac{(\mathbf{p}'^2 - \mathbf{p}^2)}{4m^2} \frac{\boldsymbol{\sigma} \cdot (\mathbf{p}' - \mathbf{p})}{m} \Bigg] \chi_\mu \,. \qquad (78)
\end{aligned}$$

and the vector part becomes

$$\begin{aligned}
&\langle \mathbf{p}', \mu', \tau' |\, \mathbf{J}_{k,\mathrm{NR-WNC}}(0)\, | \mathbf{p}, \mu, \tau \rangle = \\
&\qquad \delta_{\tau'\tau} \chi^\dagger_{\mu'} \Bigg\{ F^N_{1,\tau} \frac{\mathbf{p}' + \mathbf{p}}{2m} - \frac{1}{2m} (F^N_{1,\tau} + F^N_{2,\tau}) i\, \boldsymbol{\sigma} \times (\mathbf{p}' - \mathbf{p}) \\
&\quad + F^N_{A,\tau} \left[1 - \frac{(\mathbf{p}' + \mathbf{p})^2}{8m^2} \right] \boldsymbol{\sigma} + \frac{F^N_{A,\tau}}{4m^2} \Big[(\mathbf{p} \cdot \boldsymbol{\sigma}) \mathbf{p}' + (\mathbf{p}' \cdot \boldsymbol{\sigma}) \mathbf{p} \\
&\qquad\qquad + i (\mathbf{p} \times \mathbf{p}') \Big] + F^N_{P,\tau} \frac{(\mathbf{p}' - \mathbf{p})}{m} \frac{\boldsymbol{\sigma} \cdot (\mathbf{p} - \mathbf{p}')}{2m} \Bigg\} \chi_\mu \,. \qquad (79)
\end{aligned}$$

Note that the above formula can be also used (with the proper isospin operators and nucleon form factors) for electron scattering processes as well as for the charged-current induced reactions addressed in the next subsection.

B. Kinematics, matrix elements and observables for electron or neutrino induced deuteron breakup

The four-momentum conservation for the $e + d \to e' + p + n$ reaction in the laboratory frame reads

$$\begin{aligned}
E_e + m_D &= E'_e + E_p(\mathbf{p}_p) + E_n(\mathbf{p}_n) \\
\mathbf{p}_e = \mathbf{p}'_e + \mathbf{p}_p + \mathbf{p}_n &\equiv \mathbf{p}'_e + \mathbf{p}'_1 + \mathbf{p}'_2 \equiv \mathbf{p}'_e + \mathbf{q} \,, \qquad (80)
\end{aligned}$$

where $E_i(\mathbf{p}) \equiv \sqrt{m_i^2 + \mathbf{p}^2}$. A diagram representing kinematics of this process is shown in Fig. 1.

The phase space for the breakup reaction can be naturally described with the following variables:

1. electron scattering angle θ_e

2. energy of the outgoing electron, which for given θ_e lies in the interval $m_e \leq E'_e \leq E'^{\max}_e$. The maximal outgoing electron energy $E'^{\max}_e$ can be obtained from the condition that the total energy of the (p, n) system in the total-momentum-zero frame is not less than $m_p + m_n$:

$$\left(E_p(\mathbf{p}_p) + E_n(\mathbf{p}_n)\right)^2 - \left(\mathbf{p}_p + \mathbf{p}_n\right)^2 \geq \left(m_p + m_n\right)^2 , \tag{81}$$

which means

$$\left(E_e + m_D - E'_e\right)^2 - \left(\mathbf{p}_e - \mathbf{p}'_e\right)^2 \geq \left(m_p + m_n\right)^2 . \tag{82}$$

Inequality (82) can be analytically solved with the result

$$|\mathbf{p}'_e|^{\max} = \frac{G|\mathbf{p}_e|\cos\theta_e}{2\left(E_e + m_D\right)^2 - 2|\mathbf{p}_e|^2\cos^2\theta_e} + \frac{\left(E_e + m_D\right)\sqrt{4m_e^2|\mathbf{p}_e|^2\cos^2\theta_e + G^2 - 4\left(E_e + m_D\right)^2 m_e^2}}{2\left(E_e + m_D\right)^2 - 2|\mathbf{p}_e|^2\cos^2\theta_e} \tag{83}$$

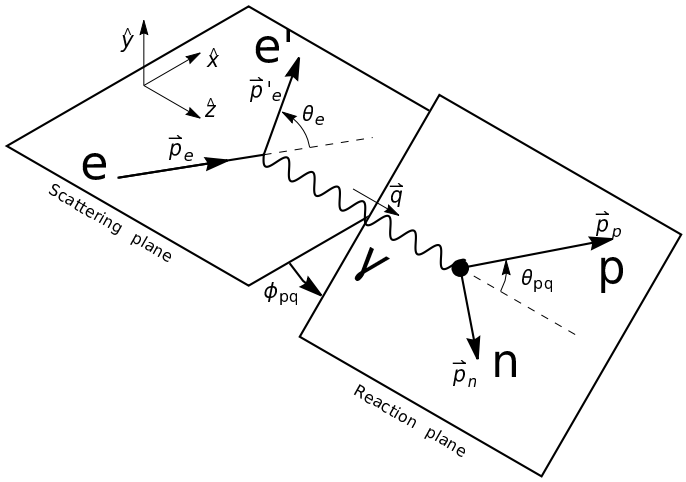

FIG. 1. Kinematics of the (e, e', p) reaction with the definitions of the kinematic variables [19].

and

$$E_e'^{\max} = \sqrt{m_e^2 + \left(|\mathbf{p}_e'|^{\max}\right)^2}\,, \tag{84}$$

where

$$G = 2m_e^2 + m_D^2 - (m_p + m_n)^2 + 2m_D\, E_e\,.$$

The three quantities $|\mathbf{p}_e|$, θ_e and $|\mathbf{p}_e'|$ define the total total energy and total three-momentum of the (p,n) system and thus its internal energy

$$E_{c.m.} = \sqrt{(\omega + m_D\,)^2 \,-\, \mathbf{q}^2} - 2m\,,$$

so we can calculate also the magnitude of the relative momentum $|\mathbf{k}|$ in the two-nucleon total-momentum-zero frame. Two additional variables, which fully determine the exclusive kinematics might be

3. polar $(0 \le \theta_k \equiv \theta_{pq} \le \pi)$ and

4. azimuthal $(0 \le \phi_k \equiv \phi_{pq} \le 2\pi)$ angle of $\mathbf{k}$ measured with respect to $\mathbf{q}$.

Obviously all the four choices can be made for any azimuthal angle of the outgoing electron momentum $(0 \le \phi_e \le 2\pi)$.

For fixed $|\mathbf{p}_e|$, θ_e, $|\mathbf{p}_e'|$ and $\mathbf{k} \equiv |\mathbf{k}|$ $(\sin\theta_k\,\cos\phi_k, \sin\theta_k\,\sin\phi_k, \cos\theta_k\,)$ we get

$$\begin{aligned}
\mathbf{p}_p &= \mathbf{k} + \left(\frac{E_p(\mathbf{k})}{M_0} + \frac{1}{M_0(M_0+E_0)}\mathbf{k}\cdot\mathbf{q}\right)\,\mathbf{q}\,,\\
\mathbf{p}_n &= -\mathbf{k} + \left(\frac{E_n(\mathbf{k})}{M_0} - \frac{1}{M_0(M_0+E_0)}\mathbf{k}\cdot\mathbf{q}\right)\,\mathbf{q}\,,
\end{aligned} \tag{85}$$

where $M_0 = E_p(\mathbf{k}) + E_n(\mathbf{k})$ and $E_0 = \sqrt{M_0^2 + |\mathbf{q}|^2}$ [20].
Very often variables of interest are

$$Q^2 = |\mathbf{q}|^2 - (E_e - E_e'\,)^2 \tag{86}$$

and

$$p_{\rm miss} = \sqrt{\left(E_n(\mathbf{p}_n)\right)^2 - m_n^2}\,. \tag{87}$$

In the practical calculations we will use approximations: we will neglect not only the neutrino but also the electron mass m_e and the difference between the proton and neutron masses, $m_p = m_n = m$. Then Eqs. (85) coincide with Eqs. (53).

The transition matrix elements for the breakup reaction are

$$\begin{aligned}
&\langle \mathbf{p}'_1, \mu'_1, \tau'_1, \mathbf{p}'_2, \mu'_2, \tau'_2, \mathbf{p}'_e, \mu'_e \| T_{\rm epn} \| \mathbf{p}_D, \mu_D, D, \mathbf{p}_e, \mu_e \rangle \\
&= -e^2 (2\pi)^3 \, {}^{(-)}\langle \mathbf{p}'_1, \mu'_1, \tau'_1, \mathbf{p}'_2, \mu'_2, \tau'_2 | J^\mu_{nuc,EM}(0) | \mathbf{p}_D, \mu_D, D \rangle \\
&\qquad \times \frac{g_{\mu\nu}}{(p'_e - p_e)^2 + i\epsilon} \langle \mathbf{p}'_e, \mu'_e | J^\nu_e(0) | \mathbf{p}_e, \mu_e \rangle \\
&\equiv -e^2 (2\pi)^3 \, \frac{1}{(2\pi)^3} \, N^\mu_{\rm epn} \left(\mathbf{p}'_1, \mu'_1, \tau'_1, \mathbf{p}'_2, \mu'_2, \tau'_2, \mathbf{p}_D, \mu_D \right) \\
&\quad \times \frac{g_{\mu\nu}}{(p'_e - p_e)^2 + i\epsilon} \frac{1}{(2\pi)^3} \, \frac{1}{\sqrt{4\, E_e \, E'_e}} L^\nu_e \left(\mathbf{p}'_e, \mu'_e, \mathbf{p}_e, \mu_e \right) \, , \qquad (88)
\end{aligned}$$

where the final two-nucleon bound state $|\mathbf{p}'_D, \mu'_D, D\rangle$ is replaced by the corresponding scattering state $|\mathbf{p}'_1, \mu'_1, \tau'_1, \mathbf{p}'_2, \mu'_2, \tau'_2\rangle^{(-)}$, which is calculated as

$$\begin{aligned}
&{}^{(-)}\langle \mathbf{p}'_1, \mu'_1, \tau'_1, \mathbf{p}'_2, \mu'_2, \tau'_2 | J^\mu_{nuc,EM}(0) | \mathbf{p}_D, \mu_D, D \rangle \\
&= \langle \mathbf{p}'_1, \mu'_1, \tau'_1, \mathbf{p}'_2, \mu'_2, \tau'_2 | J^\mu_{nuc,EM}(0) | \mathbf{p}_D, \mu_D, D \rangle \qquad (89) \\
&+ \langle \mathbf{p}'_1, \mu'_1, \tau'_1, \mathbf{p}'_2, \mu'_2, \tau'_2 | t(E + i\epsilon) G_0(E + i\epsilon) J^\mu_{nuc,EM}(0) | \mathbf{p}_D, \mu_D, D \rangle \, , \qquad (90)
\end{aligned}$$

where $E = E_e + m_D - E'_e$, $G_0(E)$ is the relativistic free two-nucleon propagator and $t(E)$ is the "boosted" t-matrix, which obeys

$$t(E; |\mathbf{q}|) = v(|\mathbf{q}|) + t(E; |\mathbf{q}|) \, G_0(E + i\epsilon) v(|\mathbf{q}|) \, , \qquad (91)$$

where $v(|\mathbf{q}|) = \sqrt{4\,(|\mathbf{k}|^2 + m^2 + 2mV) + |\mathbf{q}|^2} - \sqrt{4\,(|\mathbf{k}|^2 + m^2) + |\mathbf{q}|^2}$ is the "boosted" potential [2]. For the single-nucleon contribution in the nuclear matrix element the plane-wave part (89) is given in Eq. (A3). Various types of the rescattering parts of the nuclear matrix elements are evaluated in the appendix.

The generic formulas for any type of the cross section in terms of (88) is

$$\begin{aligned}
{\rm d}\sigma = &\frac{(2\pi)^4 E_D E_e}{\sqrt{(p_D \cdot p_e)^2 - m_D^2 m_e^2}} |\langle \mathbf{p}'_1, \mu'_1, \tau'_1, \mathbf{p}'_2, \mu'_2, \tau'_2, \mathbf{p}'_e, \mu'_e \| T_{\rm epn} \| \mathbf{p}_D, \mu_D, D, \mathbf{p}_e, \mu_e \rangle|^2 \\
&\times E(\mathbf{p}'_1) E(\mathbf{p}'_2) E'_e \, \delta^4(p_D + p_e - p'_1 - p'_2 - p'_e) \frac{{\rm d}\mathbf{p}'_1}{E(\mathbf{p}'_1)} \frac{{\rm d}\mathbf{p}'_2}{E(\mathbf{p}'_2)} \frac{{\rm d}\mathbf{p}'_e}{E'_e} \, . \qquad (92)
\end{aligned}$$

We take essentially the same steps as for elastic electron-deuteron scattering cross section to obtain in the laboratory frame [13, 21]

$$\frac{\mathrm{d}^5\sigma}{\mathrm{d}\hat{\mathbf{p}}'_e \mathrm{d}|\mathbf{p}'_e| \mathrm{d}\hat{\mathbf{p}}'_1} = \sigma_{Mott} \sum_{\text{physical } |\mathbf{p}'_1|} \frac{|\mathbf{p}'_1|^2}{\left| \frac{|\mathbf{p}'_1|}{E(\mathbf{p}'_1)} + \frac{|\mathbf{p}'_1| - |\mathbf{q}| \cos\theta_1}{E(\mathbf{p}'_2)} \right|}$$
$$\times \left(v_L R_L + v_T R_T + v_{TT} R_{TT} + v_{TL} R_{TL} \; + \; h \left(v_{T'} R_{T'} + v_{TL'} R_{TL'} \right) \right), \tag{93}$$

where we assume that polarization of the final electron is not measured and that the spin of the initial electron is parallel ($h = 1$) or antiparallel ($h = -1$) to its momentum. Note that θ_1 is the angle between $\mathbf{p}'_1$ and $\mathbf{q}$. The v_i functions are given in terms of the four momentum transfer squared Q^2 (positive), three momentum transfer squared $|\mathbf{q}|^2$, and the electron scattering angle θ_e

$$\begin{aligned}
v_L &= \frac{(Q^2)^2}{|\mathbf{q}|^4}, \\
v_T &= \frac{1}{2}\frac{Q^2}{|\mathbf{q}|^2} + \tan^2\frac{\theta_e}{2}, \\
v_{TT} &= -\frac{1}{2}\frac{Q^2}{|\mathbf{q}|^2}, \\
v_{TL} &= -\frac{1}{\sqrt{2}}\frac{Q^2}{|\mathbf{q}|^2}\sqrt{\frac{Q^2}{|\mathbf{q}|^2} + \tan^2\frac{\theta_e}{2}}, \\
v_{T'} &= \sqrt{\frac{Q^2}{|\mathbf{q}|^2} + \tan^2\frac{\theta_e}{2}}\,\tan\frac{\theta_e}{2}, \\
v_{TL'} &= -\frac{1}{\sqrt{2}}\frac{Q^2}{|\mathbf{q}|^2}\,\tan\frac{\theta_e}{2}.
\end{aligned} \tag{94}$$

The nuclear response functions R_i are

$$\begin{aligned}
R_L &= \mid N^0_{\text{epn}} \mid^2, \\
R_T &= \mid N_{\text{epn},+1} \mid^2 + \mid N_{\text{epn},-1} \mid^2, \\
R_{TT} &= 2\Re\left(N_{\text{epn},+1} N^*_{\text{epn},-1}\right), \\
R_{TL} &= -2\Re\left(N^0_{\text{epn}} (N_{\text{epn},+1} - N_{\text{epn},-1})^*\right), \\
R_{T'} &= \mid N_{\text{epn},+1} \mid^2 - \mid N_{\text{epn},-1} \mid^2, \\
R_{TL'} &= -2\Re\left(N^0_{\text{epn}} (N_{\text{epn},+1} + N_{\text{epn},-1})^*\right),
\end{aligned} \tag{95}$$

where

$$N_{\rm epn,+1} = -\frac{1}{\sqrt{2}}\left(N^1_{\rm epn} + iN^2_{\rm epn}\right) \equiv -\frac{1}{\sqrt{2}}\left(N_{{\rm epn},x} + iN_{{\rm epn},y}\right) ,$$
$$N_{\rm epn,-1} = \frac{1}{\sqrt{2}}\left(N^1_{\rm epn} - iN^2_{\rm epn}\right) \equiv \frac{1}{\sqrt{2}}\left(N_{{\rm epn},x} - iN_{{\rm epn},y}\right)$$

are spherical components of $\mathbf{N}_{\rm epn}$. The two-nucleon scattering states in $N^0_{\rm epn}$, $N_{\rm epn,+1}$ and $N_{\rm epn,-1}$ are antisymmetrized and polarizations of the hadronic states in Eq. (93) can be still chosen at will. Equation (93) is a starting point for defining target-spin independent or target-spin dependent helicity asymmetries as well as the various target analyzing powers.

The choice of individual momentum in Eq. (93) is not always convenient and often (see for example [22]) another form of the phase space factor for fixed $\mathbf{p}'_e$ is used:

$$\begin{aligned}
\rho_2 &\equiv {\rm d}\mathbf{p}'_1\,{\rm d}\mathbf{p}'_2\,\delta^4(p_D + p_e - p'_e - p'_1 - p'_2) \\
&= {\rm d}\mathbf{p}'\,{\rm d}\mathbf{k}'\left|\frac{\partial\,(\mathbf{p}'_1,\mathbf{p}'_2\,)}{\partial\,(\mathbf{p}',\mathbf{k}'\,)}\right|\,\delta^4(p_D + p_e - p'_e - p'_1 - p'_2) \\
&= {\rm d}\mathbf{p}'\,{\rm d}\mathbf{k}'\,\mathcal{N}^2(\mathbf{p}'_1,\mathbf{p}'_2)\,\delta^4(p_D + p_e - p'_e - p'_1 - p'_2) \\
&= {\rm d}\hat{\mathbf{k}}'\,\frac{1}{4}\,E\,|\mathbf{k}'|_{\rm physical}\,\mathcal{N}^2(\mathbf{p}'_1,\mathbf{p}'_2)\,, \qquad (96)
\end{aligned}$$

which leads to to

$$\begin{aligned}
\frac{{\rm d}^5\sigma}{{\rm d}\hat{\mathbf{p}}'_e{\rm d}|\mathbf{p}'_e|{\rm d}\hat{\mathbf{k}}'} &= \sigma_{Mott}\,\frac{1}{4}\,E\,|\mathbf{k}'|_{\rm physical}\,\mathcal{N}^2(\mathbf{p}'_1,\mathbf{p}'_2) \\
\times\Big(v_L R_L + v_T R_T + v_{TT} R_{TT} + v_{TL} R_{TL} \,+\, h\,(v_{T'} R_{T'} + v_{TL'} R_{TL'}\,)\Big)\,. \qquad (97)
\end{aligned}$$

Further, we calculate semi-exclusive cross sections

$$\begin{aligned}
\frac{{\rm d}^3\sigma}{{\rm d}\hat{\mathbf{p}}'_e{\rm d}|\mathbf{p}'_e|} &= \int {\rm d}\hat{\mathbf{k}}'\,\frac{{\rm d}^5\sigma}{{\rm d}\hat{\mathbf{p}}'_e{\rm d}|\mathbf{p}'_e|{\rm d}\hat{\mathbf{k}}'} \\
&= \int_0^{2\pi}{\rm d}\phi_{k'}\int_0^{\pi}{\rm d}\theta_{k'}\,\sin\theta_{k'}\,\frac{{\rm d}^5\sigma}{{\rm d}\hat{\mathbf{p}}'_e{\rm d}|\mathbf{p}'_e|{\rm d}\hat{\mathbf{k}}'}\,. \qquad (98)
\end{aligned}$$

IV. NUMERICAL RESULTS

For the reactions on the deuteron we show predictions for different processes and kinematics. For electron scattering we start with results for the elastic scattering $e + d \to e' + d'$ observables and discuss predictions for the structure functions $A(Q^2)$ and $B(Q^2)$, which constitute the differential cross section $\frac{{\rm d}\sigma^{\rm el}}{{\rm d}\hat{\mathbf{p}}'_e}(Q^2,\theta_e)$. We consider also the standard polarization observable, the deuteron tensor analyzing power T_{20}. For the breakup reaction,

$e + d \rightarrow e' + p + n$, we can calculate not only the corresponding $\frac{\mathrm{d}\sigma^{\mathrm{br}}}{\mathrm{d}\hat{\mathbf{p}}'_e}(Q^2, \theta_e)$ cross sections but also fully exclusive ones, $\frac{\mathrm{d}^5\sigma}{\mathrm{d}\hat{\mathbf{p}}'_e \mathrm{d}|\mathbf{p}'_e| \mathrm{d}\hat{\mathbf{p}}'_1}$, where $\hat{p}'_1$ denotes the direction of the outgoing nucleon momentum determined on top of the final electron momentum $\mathbf{p}'_e$. It is also very frequent that other kinematical variables, for example Q^2 or the so-called missing momentum p_{miss}, are used to define parts of the studied phase space.

In the case of neutrino-induced reactions we focus mainly on the total elastic and breakup cross sections but show also examples of the angular distributions of the cross sections.

A. Elastic electron-deuteron scattering

Elastic electron-deuteron scattering has been studied by many authors; see for example [15, 23–25]. Standard observables are the structure functions $A(Q^2)$ and $B(Q^2)$ as well as the tensor analyzing power $T_{20}(Q^2, \theta)$ at θ_{lab}= 70° [15].

The observables can be investigated for various ranges of the four-momentum transfer squared. In order to reach higher Q^2-values one has to consider a sufficiently high initial electron energy. This raises difficulties, if we want to compare results of strictly nonrelativistic calculations with the relativistic ones, since already the nonrelativistic kinematics yields results very different from the relativistic kinematics. This is shown for two basic quantities, the final electron energy and the four-momentum transfer squared in Figs. 2-3 at the initial electron energy 1 and 3 GeV. That is why our "nonrelativistic" predictions mean that in this case the nonrelativistic single-nucleon current operator and wave functions are combined with the *relativistic* kinematics.

Figure 4 shows for $Q^2 \leq 0.4$ GeV^2 that the relativistic corrections to the nonrelativistic single-nucleon current are negligible for the two deuteron form factors. In this Q^2 range it is also possible to employ the nonrelativistic kinematics for the deuteron, making thus the nuclear part of the calculation more consistent.

Data for the observables were collected in Ref. [15] and comprise many sets. For $A(Q^2)$ they include those from Refs. [26, 27, 30–37]. Data for $B(Q^2)$ come from Refs. [28–30, 35, 38, 39].

In Fig. 5 we display the structure functions $A(Q^2)$ and $B(Q^2)$ on a logarithmic scale for a broader range of Q^2-values. Since the nonrelativistic kinematics is no longer applicable, the nonrelativistic results mean in this case only the nonrelativistic single-nucleon current

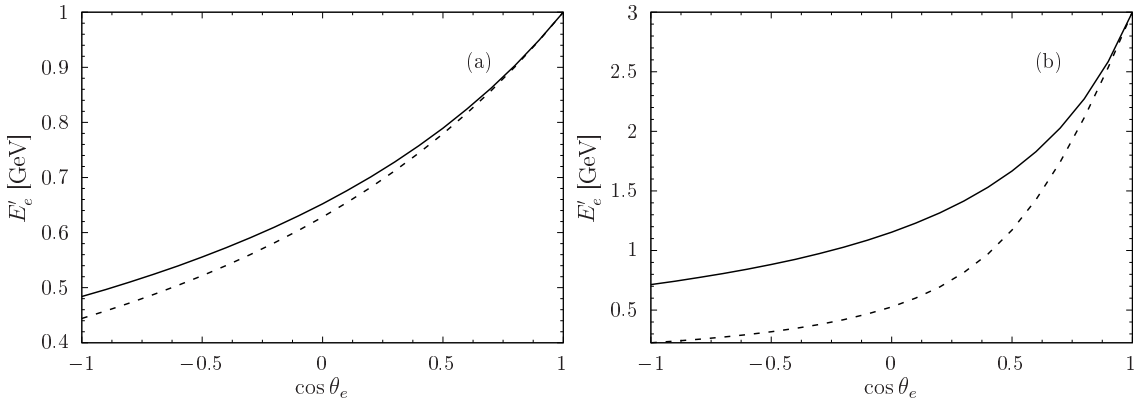

FIG. 2. The final electron energy E'_e calculated relativistically (solid line) and nonrelativistically (dashed line) as a function of the cosine of the electron scattering angle $\cos\theta_e$ for the initial electron energy E_e= 1 GeV (a) and 3 GeV (b).

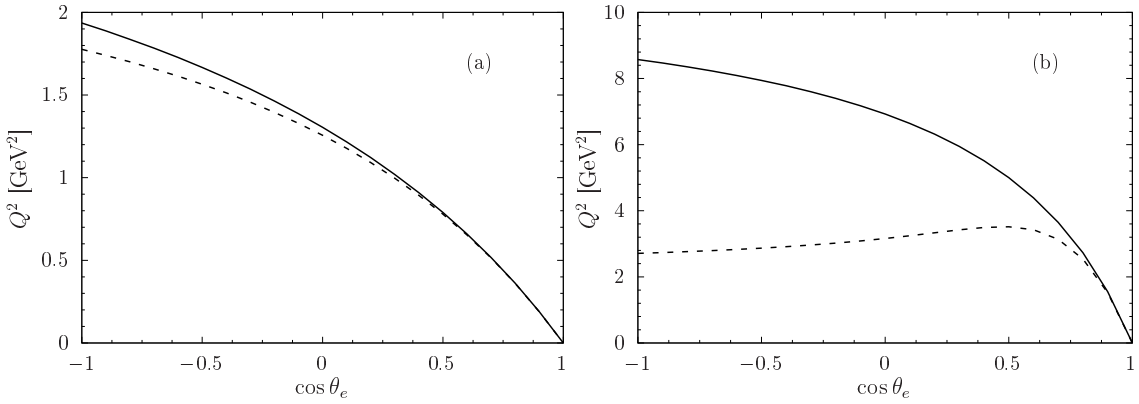

FIG. 3. Same as in Fig. 2 but for the four-momentum transfer squared, Q^2.

operator and the deuteron wave function. We show clear effects of the relativistic corrections in the single-nucleon current operator emerging at higher Q^2 values. Including these corrections actually makes the difference between the relativistic and nonrelativistic results larger. This behavior is visible for the structure function $A(Q^2)$, since the corrections affect only the charge density operator.

Without 2N contributions in the nuclear current operator we are not able to describe the data properly [15, 24, 25]. The gap between our relativistic (and thus "best") results and the data is clearly visible for the structure function $B(Q^2)$ already for lower Q^2-values.

The bulk of our results is obtained with the simple dipole parametrization of the nucleon

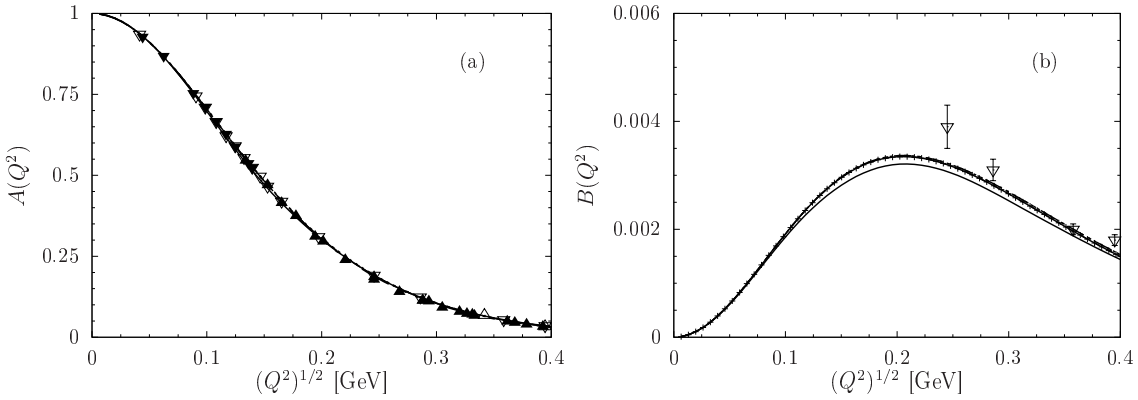

FIG. 4. The structure function $A(Q^2)$ (left panel) and $B(Q^2)$ (right panel) as a function of the square root of the absolute value of the four-momentum transfer squared, Q^2, for low Q^2-values. Various nonrelativistic predictions are compared with the relativistic result. Experimental data for (a) are from Refs. [26] (white triangles), [27] (black down triangles) and [28] (black triangles). Experimental data for (b) are from [29] (white down triangles). To be compared with Figs. 1 and 2 in Ref. [25]. The dashed line (solid line with crosses) is the structure function evaluated for non-relativistic kinematics with the non-relativistic (non-relativistic plus relativistic corrections) current operator, while the dotted (dash-dotted) line is the same quantity with relativistic kinematics and non-relativistic (non-relativistic plus relativistic corrections) current operator. Finally the solid line is the structure function evaluated fully relativistically.

electromagnetic (and also weak) form factors [12]. For the present investigation the difference between various parametrizations is not important but we checked also results obtained with the recent parametrizations from Budd, Bodek, and Arrington [9]; Kelly [10]; and Lomon [11]. For higher Q^2-values some spread between results based on various form factor parametrizations develops and is demonstrated in Fig. 6. This spread is essentially due to the difference between the predictions using the dipole parametrization [12] and the three others [9–11].

We checked also the effects of the Wigner spin rotations for these two deuteron structure functions. They are very small and predictions calculated with the Wigner D-functions replaced by the 2×2 identity matrix (not shown here) are extremely close to the complete results.

Figures 4–6 were generated choosing the initial electron energy E_e= 3 GeV and taking

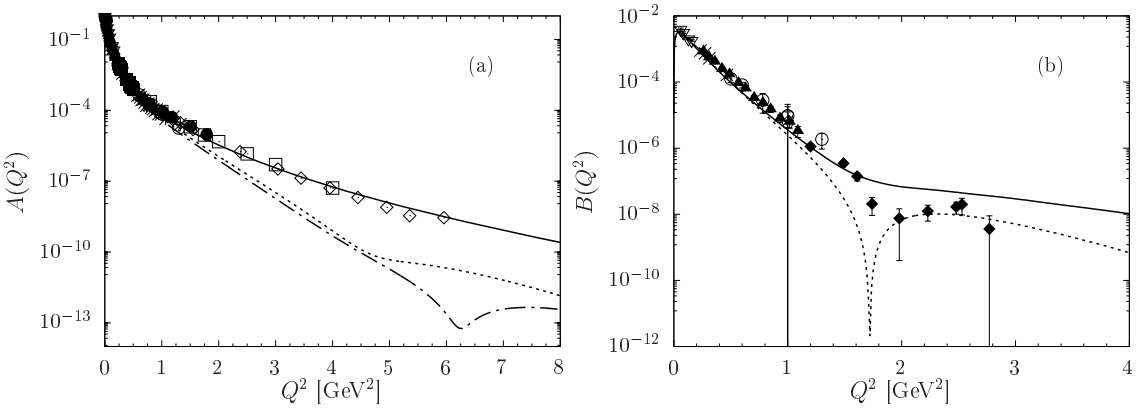

FIG. 5. The structure function $A(Q^2)$ (left panel) and $B(Q^2)$ (right panel) as a function of the absolute value of the four-momentum transfer squared, Q^2, shown on a logarithmic scale for a broader range of Q^2-values. To be compared with Figs. 9 and 10 in Ref. [15]. The used lines are the same as in Fig. 4. Experimental data are from Ref. [30] (x), [31] (*), [32] (white squares), [34] (black squares), [35] (white circles), [36] (black circles), [37] (white diamonds), [38] (black diamonds), [39] (white pentagon). The rest of the symbols for the data points has been described in Fig. 4.

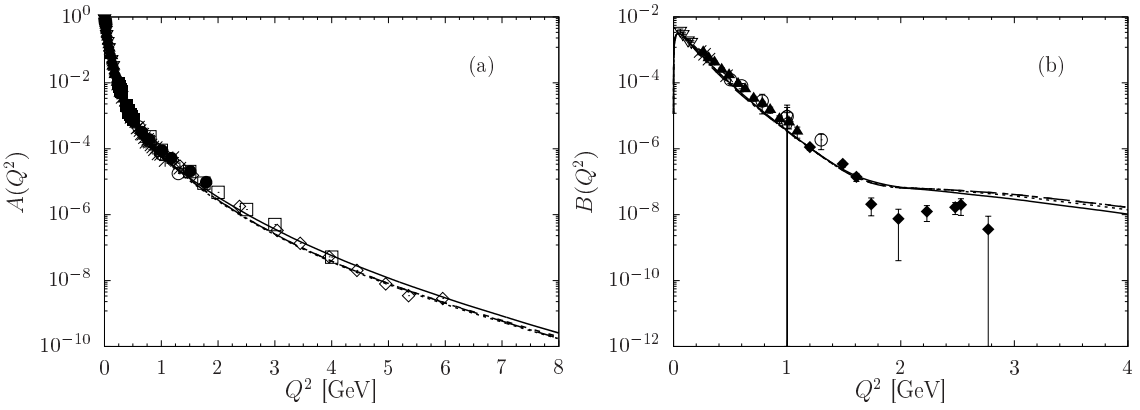

FIG. 6. The structure function $A(Q^2)$ (left panel) and $B(Q^2)$ (right panel) as a function of the absolute value of the four-momentum transfer squared, Q^2, calculated with four different parametrizations of the electromagnetic nucleon form factors. The solid line is the dipole parametrization from Ref. [12], the dashed line is from Ref. [10], the dotted line is from Ref. [11] and the dash-dotted line is from Ref. [9]. The symbols for the data points are the same as in Fig. 5.

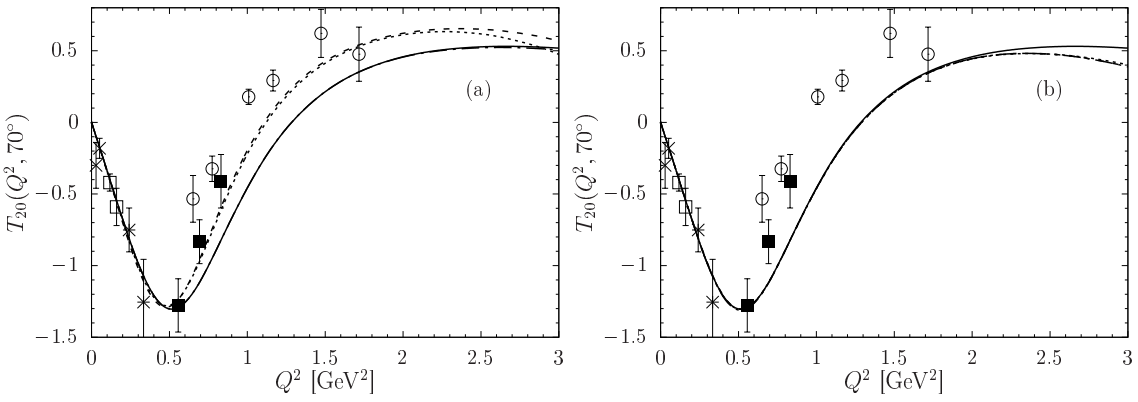

FIG. 7. The deuteron tensor analyzing power T_{20} for the electron laboratory scattering angle $\theta_e = 70^\circ$ as a function of the absolute value of the four-momentum transfer squared, Q^2. In the left panel two different nonrelativistic predictions are compared with the relativistic results. The dashed (dotted) line represents predictions obtained with the non-relativistic current operator without (with) $(p/m)^2$ corrections, while the relativistic results (relativistic results ignoring the Wigner spin rotations) are displayed with the solid (dash-dotted) line. A very small effect of the Wigner spin rotations is hardly visible even at the largest shown Q^2-values since the solid and dash-dotted lines overlap. In the right panel this polarization observable is shown for four different parametrizations of the electromagnetic nucleon form factors [12] (solid line), [9] (dash-dotted line), [10] (dashed line), and [11] (dotted line). Note that the dash-dotted, dashed and dotted lines overlap. All the calculations are based on the relativistic kinematics. Experimental data are from Refs. [40, 41] (x), [42] (*), [43] (white squares), [44] (black squares) and [45] (white circles).

a fixed step ($\frac{1}{8}^\circ$) in the electron scattering angle. In this way we could cover the selected range of the Q^2-values.

The third observable usually studied for elastic electron-deuteron scattering is the deuteron tensor analyzing power T_{20}. It is investigated at fixed laboratory electron scattering angle $\theta_e = 70^\circ$ as a function of Q^2. Thus it is sufficient to change the initial electron energy to generate this Q^2-dependence. We took a 2-MeV step up to 2 GeV.

In the left panel of Fig. 7 it is shown that up to approximately 0.4 GeV^2 all the predictions coincide but for the higher Q^2-values the relativistic results are significantly below the two nonrelativistic calculations. Relativistic $(p/m)^2$ corrections to the single-nucleon current operator become important at $Q^2 = 2$ GeV^2. Still the effect of the Wigner spin

rotations is hardly visible, even at Q^2= 3 GeV^2. In the right panel T_{20} is shown for the four parametrizations of the electromagnetic nucleon form factors [9–12]. Up to approximately Q^2= 1.7 GeV^2 all the four curves overlap, but for the higher Q^2 values the prediction obtained with the simple dipole parametrization from Ref. [12] differs from the other three, which remain essentially indistinguishable.

While consistent relativistic calculations are possible by computing independent current matrix elements and generating the rest using covariance, the comparison of the calculations with data points to a need for two-body currents. Note however, that also in this case we employ the relativistic kinematics in the nonrelativistic calculations.

B. Exclusive deuteron electrodisintegration

The $e + d \to e' + p + n$ reaction offers more possibilities than the corresponding elastic scattering process due to the richer phase space. On top of the electron parameters (E_e, θ_e, E'_e) additional quantities are needed to fix the exclusive kinematics. Due to very small values of the cross sections in the so-called point-like geometry, they are very hard to measure in a realistic experiment but we decided to demonstrate essential features of the exclusive cross sections. In Fig. 8(a) we choose (arbitrary) initial electron energy E_e= 800 MeV and consider two electron kinematics. In the first one (θ_e= 38.7° E'_e= 635.3 MeV), where $E_{c.m.}$= 100 MeV and $|\mathbf{q}|$= 500 MeV, there is no restriction on the angle θ_p between the outgoing proton momentum $\mathbf{p}_p$ and $\mathbf{q}$, so this angle can be chosen to label the exclusive kinematics. We restrict ourselves to the case, where either ϕ_{pq}= 0 (negative θ_p) or ϕ_{pq}= 180° (positive θ_p). There are regions, where the rescattering effects given by the difference between the solid and dotted lines (relativistic calculations) or the dashed and dash-dotted lines (nonrelativistic results) are very strong. In particular in the very proton knockout peak rescattering effects reduce the values of the *plane wave* (obtained without rescattering contribution) cross sections. Also here we see clear differences between the relativistic and nonrelativistic predictions.

In the second kinematics considered in Fig. 8(b) (θ_e= 106.5°, E'_e= 414.4 MeV) the internal two-nucleon energy $E_{c.m.}$= 150 MeV is much smaller than the magnitude of the three-momentum transfer $|\mathbf{q}|$= 1000 MeV. For such electron parameters $0 \leq \theta_p < 90°$ and for each θ_p there are two physical solutions. In this case the so-called "missing" momentum, p_{miss}, the

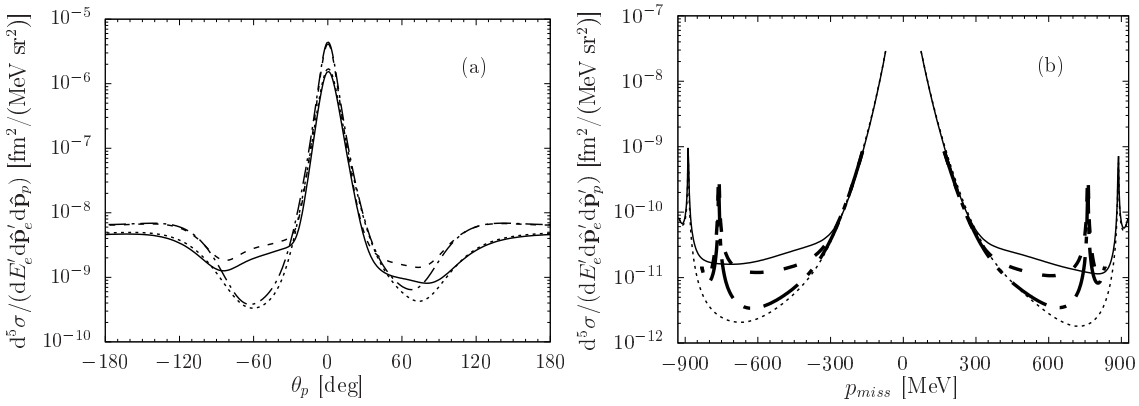

FIG. 8. Predictions for the five fold differential cross section $\mathrm{d}^5\sigma/(\mathrm{d}\hat{\mathbf{p}}'_e\mathrm{d}E'_e\mathrm{d}\hat{\mathbf{p}}_p)$ for the exclusive $^2\mathrm{H}(e,e'p)n$ reaction at fixed outgoing electron parameters ((a) E_e= 800 MeV, θ_e= 38.7°, E'_e= 635.3 MeV, (b) (E_e= 800 MeV, θ_e= 106.5°, E'_e= 414.4 MeV)) with (a) $E_{c.m.}$= 100 MeV and $|\mathbf{q}|$= 500 MeV, (b) $E_{c.m.}$= 150 MeV and $|\mathbf{q}|$= 1000 MeV, shown as a function of (a) the polar angle of the outgoing proton momentum, (b) the magnitude of the momentum of the undetected (here neutron) nucleon ("missing" momentum). Negative values of θ_p or p_{miss} correspond to ϕ_{pq}= 0 and their positive values to ϕ_{pq}= 180°. The dotted (solid) line represents the relativistic results without (including) the rescattering contribution. The corresponding nonrelativistic predictions without (with) the rescattering part are shown with the dash-dotted (dashed) line.

magnitude of the momentum of the undetected neutron, is convenient to label the exclusive kinematics. The physical ranges of θ_p and p_{miss} are quite different in the nonrelativistic and relativistic calculations, which makes the comparison more difficult. The sharp peaks correspond to the maximal θ_p values, where the phase space factor becomes singular. Small p_{miss} values coincide with the proton knockout peak and here the rescattering effects are very small.

C. The cross section in the $^2\mathrm{H}(e,e'p)$ process at low energy transfer and close to threshold

In this subsection we consider the cross section for the $^2\mathrm{H}(e,e'p)$ reaction at a low initial electron energy and momentum transfer for the measurement reported in Ref. [46]. As in many other papers by H. Arenhövel (see for example [19, 22]) the data are shown in a

"mixed" representation: the electron energies and the electron scattering angle are defined in the laboratory frame but the proton angles are given in the two-nucleon c.m. frame. It is then natural to start from the cross section $\mathrm{d}^5\sigma/\left(\mathrm{d}E'_e \mathrm{d}\hat{\mathbf{p}}'_e \mathrm{d}\hat{\mathbf{k}}\right)$ defined in Eq. (97).

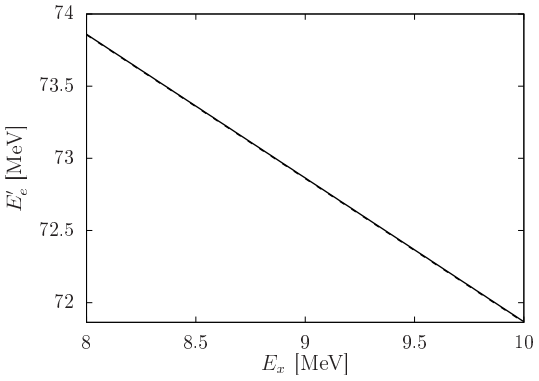

FIG. 9. The final electron energy E'_e as a function of the excitation energy E_x in the $^2\mathrm{H}(e,e',p)$ reaction calculated relativistically and nonrelativistically for the initial electron energy E= 85 MeV and the electron scattering angle θ_e= 40°. The two curves fully overlap.

The excitation energy used in [46] is the kinetic energy in the two-nucleon c.m. frame and is uniquely related to the final electron energy. In the relativistic case the connection reads

$$E'_e = \frac{{E_x}^2 + 4E_x m - 2E_e m_D - {m_D}^2 + 4m^2}{2(E_e \cos\theta_e - E_e - m_D)}$$

and is in fact more complicated for the nonrelativistic kinematics

$$E'_e = \frac{1}{\sqrt{2}}\left(8E_e m - 8m(E_x - m_D + m) - {E_e}^2 + E_e(E_e \cos 2\theta_e - 8m\cos\theta_e)\right)^{1/2} + E_e\cos\theta_e - 2m\,.$$

For this kinematics we do not seek any visible relativistic effects, since already the connection between the excitation energy E_x and the outgoing electron energy E'_e shown in Fig. 9 suggests that nonrelativistic framework should be fully adequate. We simply check that at low energies and momenta our relativistic framework is consistent with the calculations performed for example in Refs. [47, 48].

To compare our predictions with the cross section measured in the finite excitation energy bin [46] we calculated numerically the following integral

$$\frac{\mathrm{d}^4\sigma}{\mathrm{d}\hat{\mathbf{p}}'_e \mathrm{d}\hat{\mathbf{k}}} = \int\limits_{E'^{\min}_e}^{E'^{\max}_e} \mathrm{d}E'_e \, \frac{\mathrm{d}^5\sigma}{\mathrm{d}E'_e \mathrm{d}\hat{\mathbf{p}}'_e \mathrm{d}\hat{\mathbf{k}}}\,.$$

Figure 10 shows our predictions calculated with the single-nucleon current. The agreement with the data is reasonable, which means that this low-energy observable is not sensitive to the details of the current operator - the cross section is dominated by the charge density part. However, as noted in Ref. [46], the separation of various parts in the cross section would reveal true drawbacks of the theoretical framework. Measurements at low energies, providing more detailed observables, can be really used to test important dynamical ingredients.

D. The semi-exclusive cross sections in the $^2\mathrm{H}(e,e')$ process

The semi-exclusive process, where only the final electron is detected, still allows one to vary independently the energy and the magnitude of the three-momentum transfer for fixed initial electron energy. The values of the cross sections are much higher than in the exclusive case and many measurements (see for example [49–51]) focused especially on broad

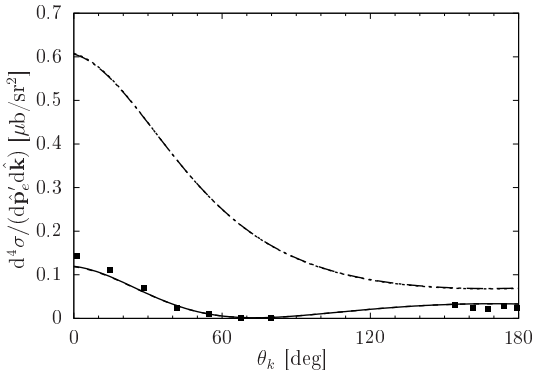

FIG. 10. The four fold differential cross section $\mathrm{d}^4\sigma/\left(\mathrm{d}\hat{\mathbf{p}}'_e\mathrm{d}\hat{\mathbf{k}}\right)$ of the $^2\mathrm{H}(e,e'p)$ reaction at E= 85 MeV for an excitation energy bin 8 MeV $\leq E_x \leq$ 10 MeV of the breakup spectra as a function of the polar proton emission angle θ_k defined with respect to the three-momentum transfer in the two-nucleon c.m. frame (the same as θ_{pq} in Fig. 1). The solid (dashed) line represents the calculation for the cross section with all (*plane wave*) contributions for the fully relativistic calculations. The dotted (dash-dotted) line represents the calculation for the cross section with all (*plane wave*) contributions for the non-relativistic calculations. Note that the plane wave results (upper curves) of the nonrelativistic and relativistic calculations overlap, as expected. The same is true for the full predictions (lower curves). The data come from Ref. [46].

maxima, which appear for the quasi-elastic scattering domain in the (θ_e, E'_e) plane, where the magnitude of the three-momentum transfer $|\mathbf{q}|$ and the energy transfer ω are related by $|\mathbf{q}|^2 \approx 2m\omega$ with m being the nucleon mass. The cross section in this region is dominated by the single-nucleon current operator, which means that our framework should give reliable predictions for such kinematics.

In Ref. [52] a rich data set for the $\mathrm{d}^3\sigma/\left(\mathrm{d}E'_e \mathrm{d}\hat{\mathbf{p}}'_e\right)$ differential cross sections (and the derived response functions) is compared with Arenhövel and Leidemann's predictions as well as with the results obtained by Laget. Here, in Figs. 11-13 we show our results corresponding to Figs. 8-10 in [52], restricting ourselves to the cross sections, although we could also calculate the nuclear response functions R_L and R_T.

As before all of our calculations are performed neglecting two-nucleon contributions to the nuclear current operator. The figures show mainly the quasi-elastic peak where these contributions should remain small. There is only a slight but visible shift between the positions of the relativistic and nonrelativistic quasi-elastic peak. We see also the characteristic enhancement of the cross sections shown by *full* calculations (including two-nucleon final state interactions) close to the threshold (left slopes), where the internal two-nucleon energy is very small. This feature is definitely supported by the data and absent in the plane wave based (*PW*) results. On right slopes and for large energy transfers, where the internal two-nucleon energy exceeds the pion mass, new channels (pion production, isobar Δ excitation) are open, which cannot be described by our theory.

Despite the incompleteness of our approach, the obtained data description is very good. That is observed especially for the energy transfers corresponding to the internal two-nucleon energies smaller than the pion mass. In all the eleven cases the relativistic predictions describe the experimental data better than the nonrelativistic ones.

E. An excursion into polarization observables

So far we have dealt mainly with the unpolarized cross sections. The investigations in this subsection are inspired by Sabine Jeschonnek and J. W. Van Orden's paper [53]. The authors investigated four polarization observables, A_d^V, A_d^T, A_{ed}^V, and A_{ed}^T. The experimental data for these quantities were presented for example in Ref. [54]. The cross section for the

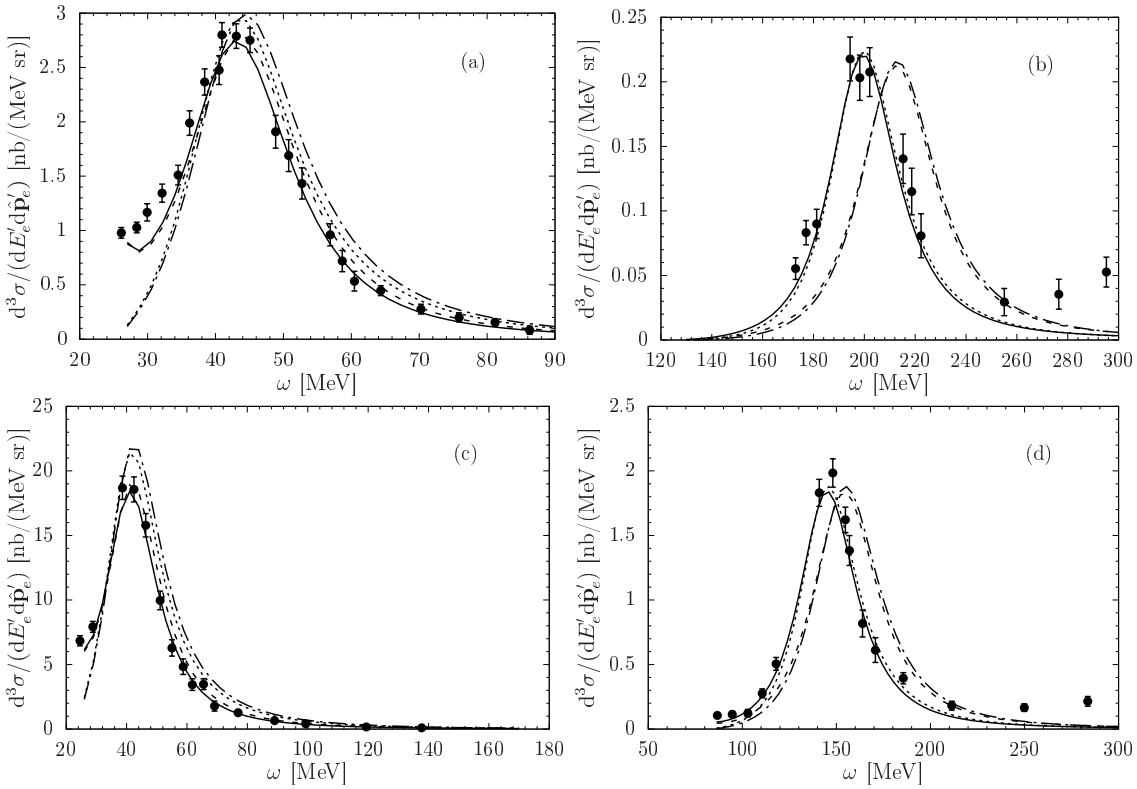

FIG. 11. Results of the nonrelativistic *plane wave* (dash-dotted line) and *full* (dashed line) calculations as well as the relativistic *plane wave* (dotted line) and *full* predictions (solid line) for the semi-exclusive cross section $\mathrm{d}^3\sigma/(\mathrm{d}E'_e\mathrm{d}\hat{\mathbf{p}}'_e)$ are shown as a function of the energy transfer ω. The sequence of subfigures follows Fig. 8 in Ref. [52].

$\overrightarrow{^2\mathrm{H}}(\vec{e},\mathrm{e'p})\mathrm{n}$ reaction (polarized beam and target) can be expressed as [53]

$$\sigma = \sigma_0 \left[1 + \sqrt{\frac{3}{2}} p_z \left(A_d^V + h A_{ed}^V \right) + \sqrt{\frac{1}{2}} p_{zz} \left(A_d^T + h A_{ed}^T \right) \right] , \tag{99}$$

where σ_0 is the unpolarized cross section, p_z and p_{zz} are the vector and tensor polarizations of the deuteron target. The same can be written in terms of the tensor polarization coefficients t_{10} and t_{20}:

$$\sigma = \sigma_0 \left[1 + t_{10} \left(A_d^V + h A_{ed}^V \right) + t_{20} \left(A_d^T + h A_{ed}^T \right) \right] . \tag{100}$$

Equations (99) and (100) are derived from the general density matrix $\rho = \rho_e \otimes \rho_d$, which is a tensor product of the electron matrix ρ_e (h is the electron helicity)

$$\rho_e = \frac{1}{2} \begin{pmatrix} 1+h & 0 \\ 0 & 1-h \end{pmatrix} \tag{101}$$

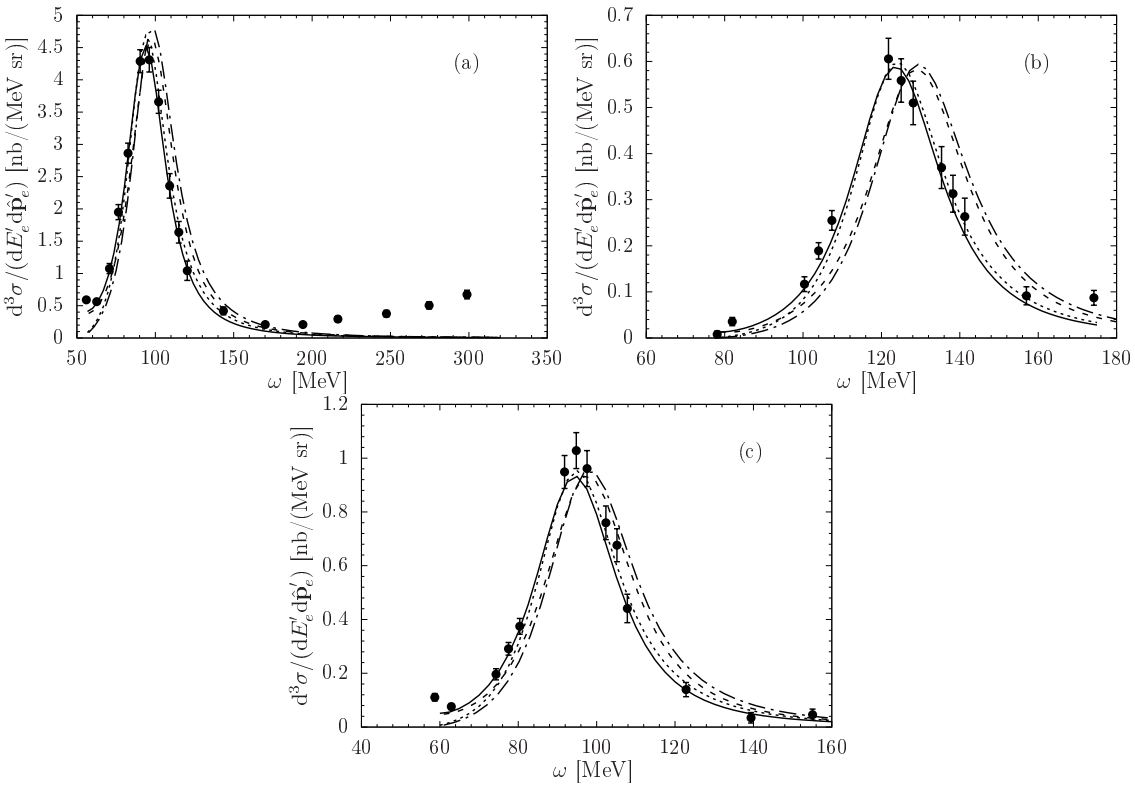

FIG. 12. The same as in Fig. 11 but for the configurations from Fig. 9 in Ref. [52].

and the deuteron matrix ρ_d

$$\rho_d = \begin{pmatrix} \frac{1}{3}\left(\sqrt{\frac{3}{2}}t_{10} + \frac{t_{20}}{\sqrt{2}} + 1\right) & -\frac{{t_{11}}^* + {t_{21}}^*}{\sqrt{6}} & \frac{{t_{22}}^*}{\sqrt{3}} \\ -\frac{t_{11}+t_{21}}{\sqrt{6}} & \frac{1}{3}\left(1 - \sqrt{2}t_{20}\right) & -\frac{{t_{11}}^* - {t_{21}}^*}{\sqrt{6}} \\ \frac{t_{22}}{\sqrt{3}} & -\frac{t_{11}-t_{21}}{\sqrt{6}} & \frac{1}{3}\left(-\sqrt{\frac{3}{2}}t_{10} + \frac{t_{20}}{\sqrt{2}} + 1\right) \end{pmatrix}, \qquad (102)$$

assuming axially symmetric deuteron target polarization – the most typical experimental situation. (In Eqs. (99)-(100) the axis of symmetry is the z-axis.)

The electron parameters used in Ref. [53] lead to $E_{c.m.}$ energies, which exceed the pion mass and do not allow us to perform our *full* calculations. For example those of Figs. 2 and 8 (E_e= 5.5 GeV, Q^2= 2 GeV^2, $x \equiv Q^2/(2m\omega)$= 1) yield $E_{c.m.} \approx 0.47$ GeV. We compared only our *plane wave* results with the PWIA predictions shown in Figs. 2, 3 and 8 in Ref. [53] and obtained very similar results (not shown).

Instead we decided to make our *full* calculations for a kinematics close to the settings used in NIKHEF experiments [55]: E_e= 565 MeV, θ_e= 35 degree and E'_e= 376 MeV. This choice leads to $E_{c.m.} \approx 159$ MeV, thus somewhat above the pion production threshold but

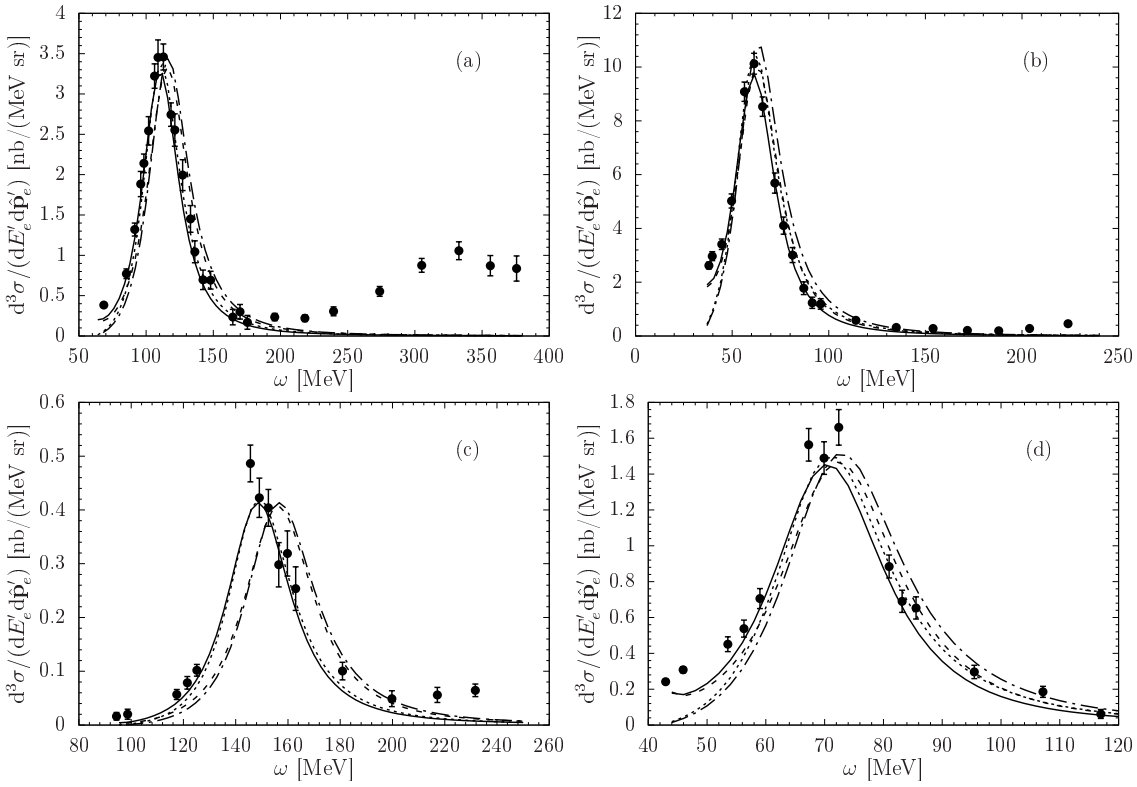

FIG. 13. The same as in Fig. 11 but for the configurations from Fig. 10 in Ref. [52].

the magnitude of the three-momentum transfer is rather small (approx. 335.5 MeV). Once the electron arm is fixed, we deal with two-body kinematics and can label exclusive events by specifying additionally the polar and azimuthal angles θ_{pq} and ϕ_{pq} of the outgoing proton momentum. These kinematical variables are defined in the two-nucleon c.m. frame (see Fig. 1).

In Figs. 14-17 we show our predictions for A_d^V, A_d^T, A_{ed}^V, and A_{ed}^T as functions of θ_{pq} for several values of ϕ_{pq}. Actually we put together results for $\phi_{pq} = x$ and $\phi_{pq} = x + 180\,\mathrm{deg}$, so $\theta_{pq} > 180\,\mathrm{deg}$ at $\phi_{pq} = x$ is to be understood as $360\,\mathrm{deg} - \theta_{pq}$ at $\phi_{pq} = x + 180\,\mathrm{deg}$. The deuteron polarization axis is chosen parallel to the three-momentum transfer $\mathbf{q}$.

Note that the polarization observables show additionally some symmetry properties. In particular A_d^V and A_{ed}^T are equal zero for ϕ_{pq}= 0 or 180 deg (not shown). The *plane wave* predictions for A_d^V and A_{ed}^T are identically zero, regardless of ϕ_{pq}. Also the non-vanishing *plane wave* results for A_d^T and A_{ed}^V are quite different from the corresponding *full* predictions. Actually the difference between the nonrelativistic and relativistic results is more pronounced for the *plane wave* calculations.

For the same "NIKHEF" electron kinematics we calculated also the more often considered deuteron analyzing powers iT_{11}, T_{20}, T_{21} and T_{22}. They are displayed in Figs. 18-21, respectively. We see in Fig. 18 that, as expected, iT_{11} is zero in the *plane wave* approximation. For the chosen electron kinematics the differences between the relativistic and nonrelativistic predictions are visible but not very strong both for the *plane wave* and *full* results. Generally, the spread between the *plane wave* and *full* results is much more pronounced, although for some of the analyzing powers there are angular regions, where all the fours curves nearly overlap.

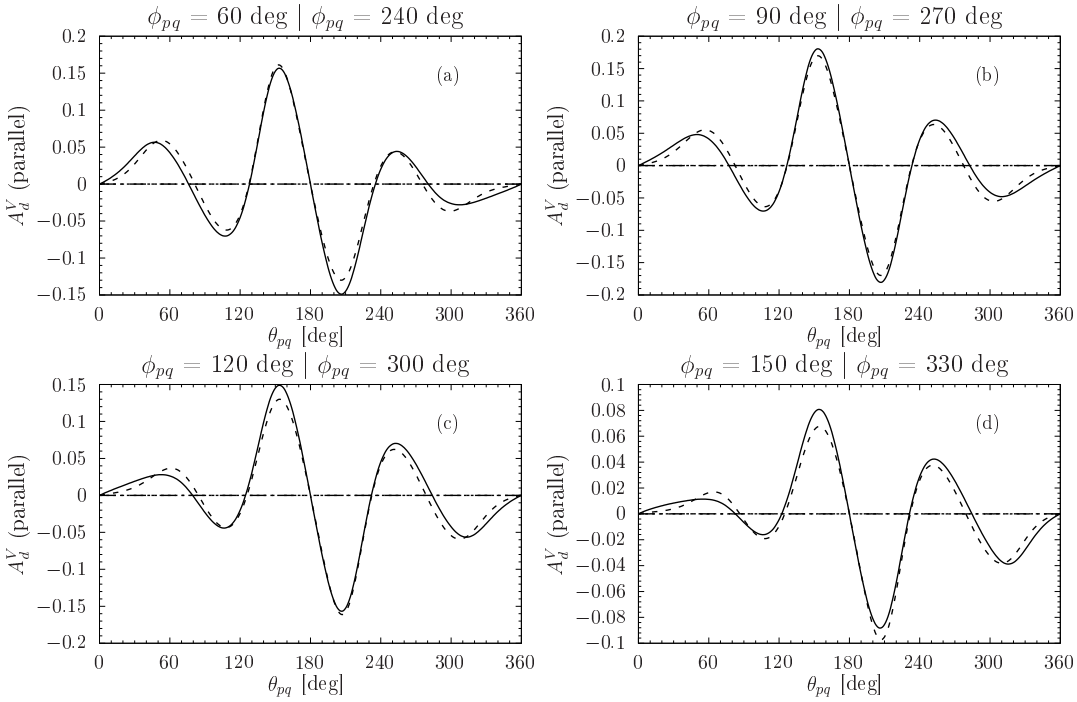

FIG. 14. Predictions for A_d^V at the "NIKHEF" kinematics for selected values of the azimuthal angle ϕ_{pq} as functions of the polar angle θ_{pq} for the deuteron polarization axis parallel to the three-momentum transfer. The solid (dotted) line represents the results with (without) the contribution of the rescattering term calculated relativistically. The dashed (dash-dotted) line represents the results with (without) the contribution of the rescattering term and calculated within the non-relativistic treatment. For this observable both *plane wave* results are identically zero.

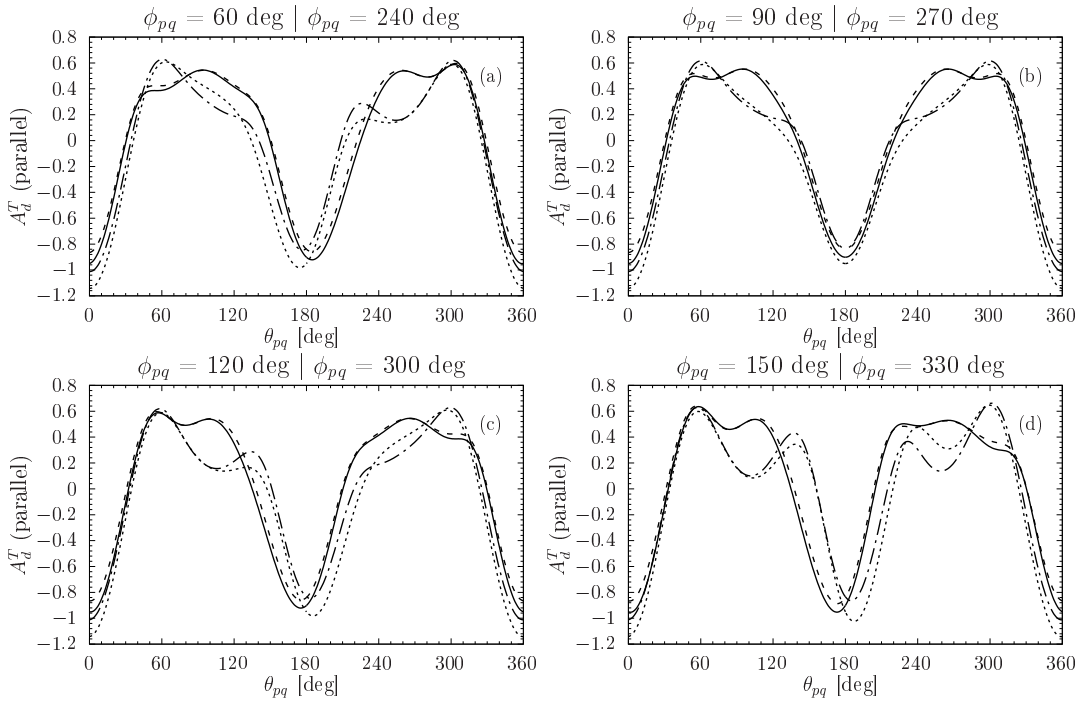

FIG. 15. Same as in Fig. 14 for A_d^T.

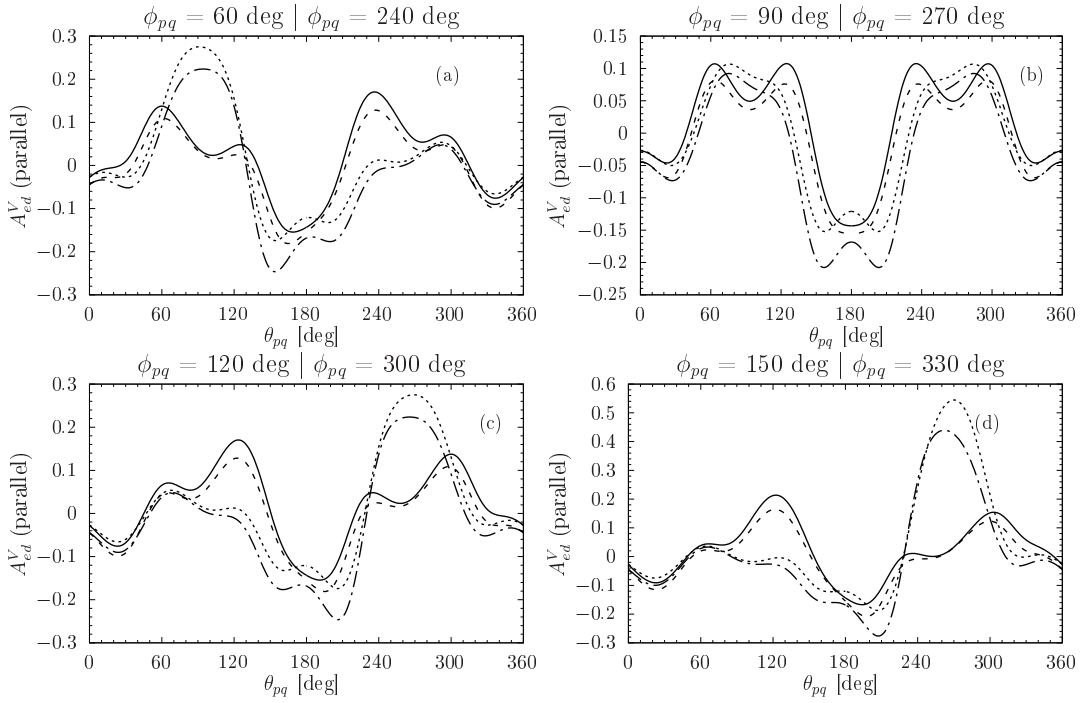

FIG. 16. Same as in Fig. 14 for A_{ed}^V.

F. Dealing with "$Q^2 - p_{miss}$" kinematics in electron induced breakup of ^{2}H

1. *Unpolarized cross sections*

In order to make transition from $\mathrm{d}^5\sigma/\left(\mathrm{d}\hat{\mathbf{p}}'_e \mathrm{d}E'_e \mathrm{d}\hat{\mathbf{k}}\right)$ to the often experimentally regarded $\mathrm{d}^2\sigma/\left(\mathrm{d}Q^2\,\mathrm{d}p_{\mathrm{miss}}\right)$ we employ the relation

$$Q^2 \approx 4E_e\,E'_e\,\sin^2\frac{\theta_e}{2}\,,$$

from which it is clear that one Q^2 value can be obtained taking various $(E'_e\,,\theta_e)$ pairs. Next, we take finite bins in Q^2 and p_{miss}, scanning the whole four dimensional parameter space to see, which combinations of $(\theta_e, E'_e, \theta_k, \phi_k\,)$ lead to required Q^2 and p_{miss} bins.

A similar procedure is often used in experiments (see for example Ref. [56]), where additionally requirements given by the experimental set-up need to be taken into account. The experimental electron kinematics from Ref. [56] cannot be used in our *full* calculations so we prepared an example for the initial electron energy E_e= 500 MeV and chose four Q^2 intervals: $(0.0875, 0.1125)\,\mathrm{GeV}^2$, $(0.175, 0.225)\,\mathrm{GeV}^2$, $(0.35, 0.45)\,\mathrm{GeV}^2$, and $(0.525, 0.675)\,\mathrm{GeV}^2$. For each Q^2 interval we proceeded in the following way: we took 100 uniformly distributed θ_e points such that $0 < \theta_e(i) < \pi$. For each $\theta_e(i)$ we calculated the kinematically allowed

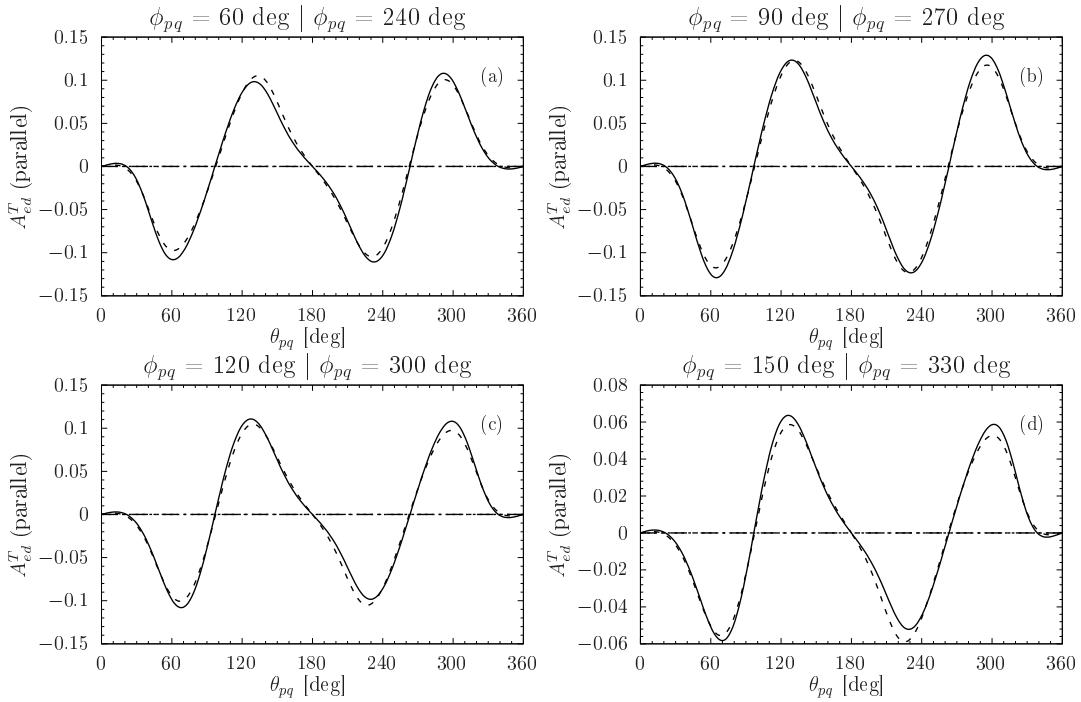

FIG. 17. Same as in Fig. 14 for A^T_{ed}.

range of the outgoing electron energies such that Q^2 fell into the desired interval. The number of the E'_e points depended on the length of this interval and varied from 1 to 100. Then for each $(E_e, \theta_e(i), E'_e(j))$ set we ran a double loop over 72 $\theta_k(l)$ and 36 $\phi_k(n)$ values (again uniformly distributed from 0 to π and from 0 to 2π, respectively) and generated the differential cross section $\mathrm{d}^5\sigma / \left(\mathrm{d}\hat{\mathbf{p}}'_e \mathrm{d}E'_e \mathrm{d}\hat{\mathbf{k}}\right)$. The values of this cross section (calculated just with the plane wave approximation or including also final state interactions) were written to a file together with the complete integral weight, which was

$$2\pi\ \Delta\theta_e(i)\ \sin\left(\theta_e(i)\right)\ \Delta E'_e(j)\ \Delta\theta_k(l)\ \sin\left(\theta_k(l)\right)\ \Delta\phi_k(n)$$

and with the value of the missing momentum (the magnitude of the neutron momentum). During computations for each Q^2 interval we created a file with several millions lines but that allowed us to sort these "events" according to the p_{miss} value and sum up all contributions

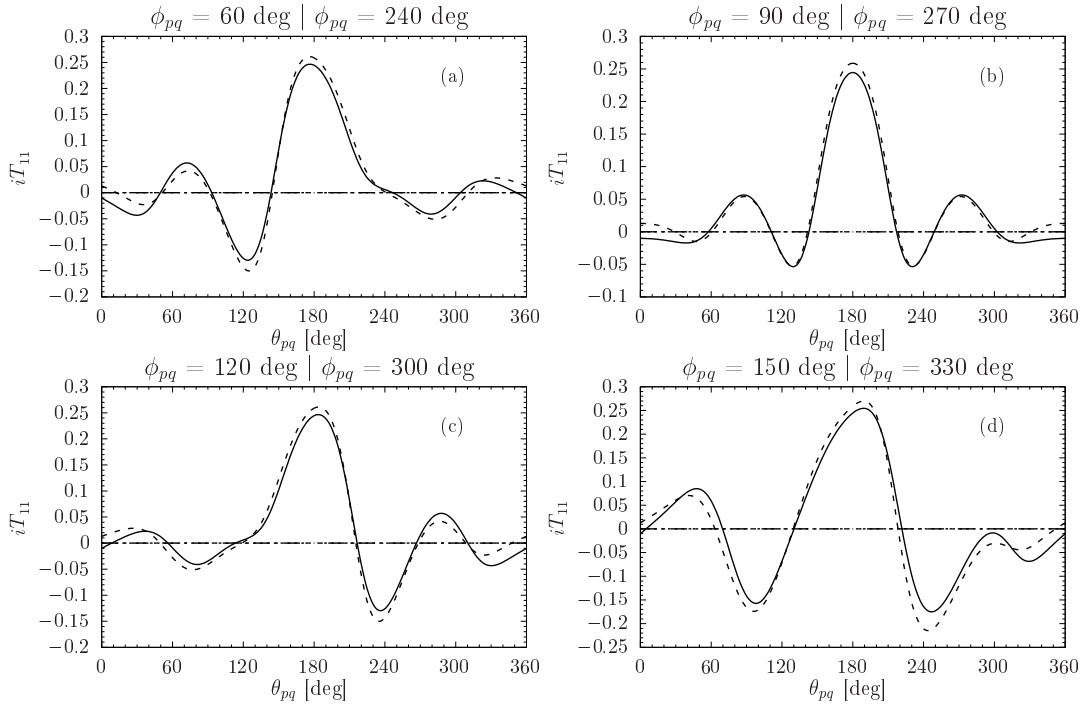

FIG. 18. Predictions for the deuteron vector analyzing power iT_{11} at the "NIKHEF" kinematics for selected values of the azimuthal angle ϕ_{pq} as functions of the polar angle θ_{pq}. Lines are the same as in Fig. 14.

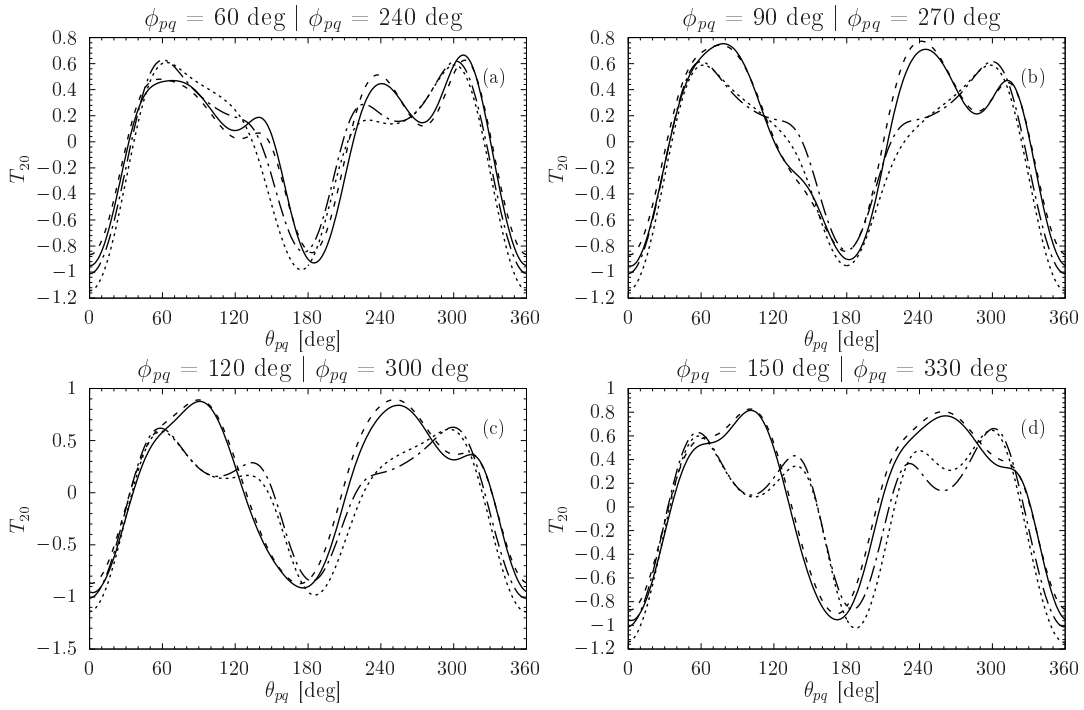

FIG. 19. The same as in Fig. 18 for the deuteron tensor analyzing power T_{20}.

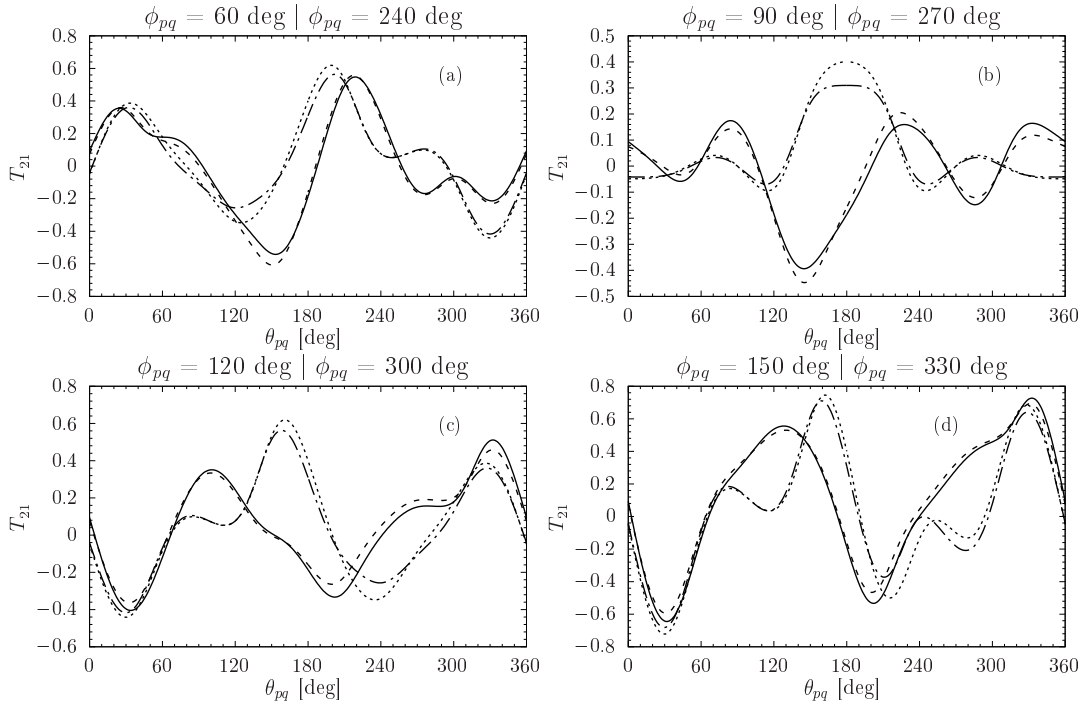

FIG. 20. The same as in Fig. 18 for the deuteron tensor analyzing power T_{21}.

belonging to a desired interval of the $\Delta p_{\rm miss}$ length. In this manner we obtained

$$\left\langle \frac{\mathrm{d}^2\sigma}{\mathrm{d}Q^2\mathrm{d}p_{\rm miss}} \right\rangle \equiv \int\limits_{Q^2_{min}}^{Q^2_{max}} \mathrm{d}Q^2 \int\limits_{\bar{p}_{\rm miss}-\frac{1}{2}\Delta p_{\rm miss}}^{\bar{p}_{\rm miss}+\frac{1}{2}\Delta p_{\rm miss}} \mathrm{d}p_{\rm miss}\, \frac{\mathrm{d}^2\sigma}{\mathrm{d}Q^2\mathrm{d}p_{\rm miss}}\,,$$

which will be then presented as a function of $\bar{p}_{\rm miss}$. It turned out that $E_{c.m.}$ values for the $Q^2 \in (0.0875, 0.1125)\,\mathrm{GeV}^2$ and $Q^2 \in (0.175, 0.225)\,\mathrm{GeV}^2$ intervals exceed by far the pion mass so we restrict ourselves to the two other cases $Q^2 \in (0.35, 0.45)\,\mathrm{GeV}^2$ and $Q^2 \in (0.525, 0.675)\,\mathrm{GeV}^2$, see Figs. 22 and 23. For these two Q^2 intervals we investigated $\left\langle \frac{\mathrm{d}^2\sigma}{\mathrm{d}Q^2\mathrm{d}p_{\rm miss}} \right\rangle$ under some kinematical dependencies calculated with two different $\Delta p_{\rm miss}$: 0.05 and 0.025 GeV. Since the kinematics at these Q^2 values is definitely relativistic, we show only our relativistic predictions. For $Q^2 \in (0.35, 0.45)\,\mathrm{GeV}^2$ the *full* results are very close to the *plane wave* predictions but for $Q^2 \in (0.525, 0.675)\,\mathrm{GeV}^2$ the two types of calculations yield different results for $p_{miss} \gtrsim 0.1$ GeV.

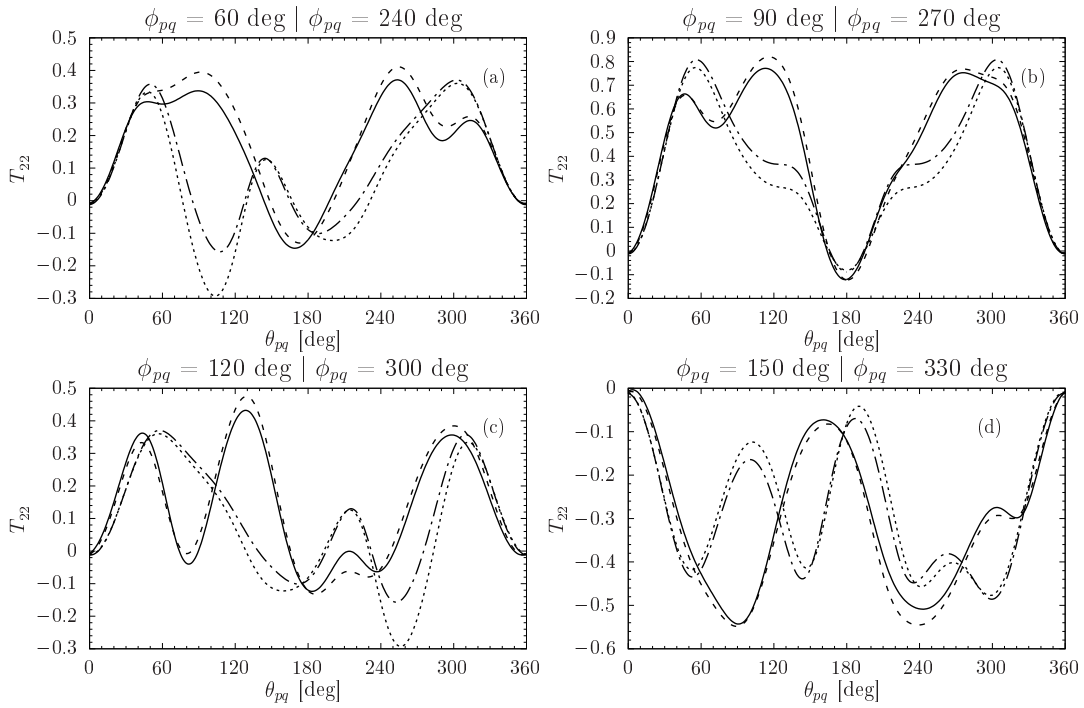

FIG. 21. The same as in Fig. 18 for the deuteron tensor analyzing power T_{22}.

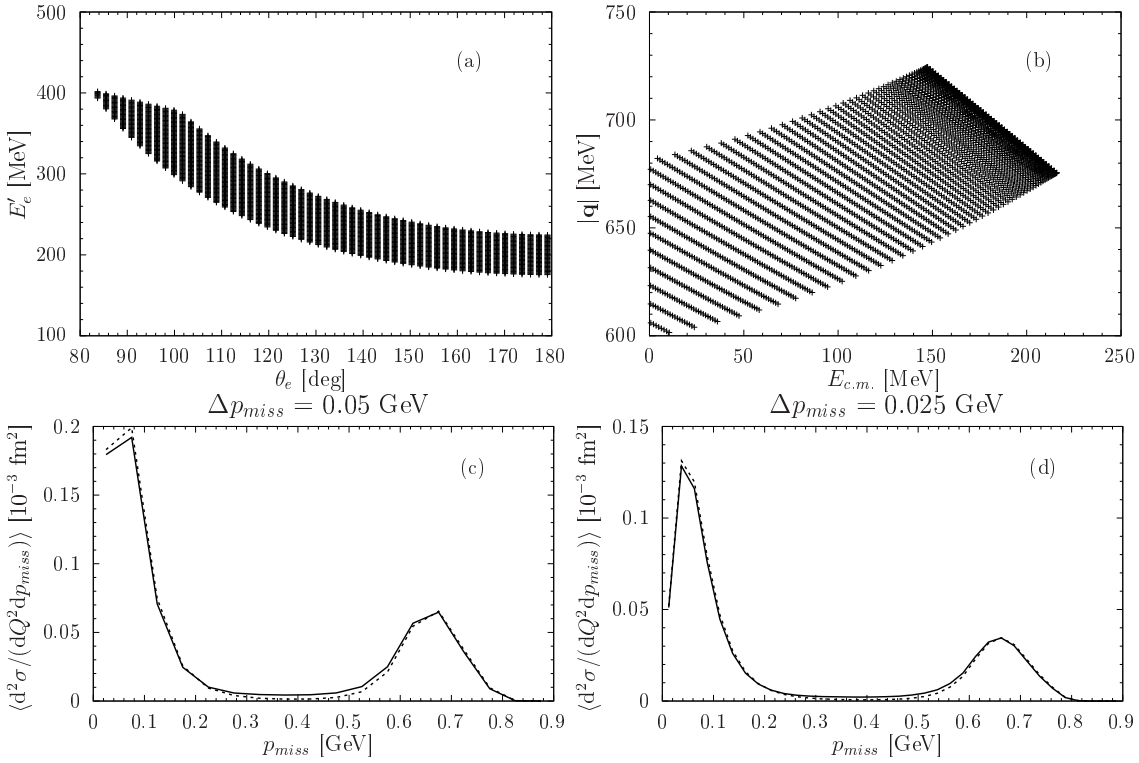

FIG. 22. Kinematical regions in the (θ_e, E'_e) (a) and $(E_{c.m.}, |\mathbf{q}|)$ (b) planes for $0.35\,\mathrm{GeV}^2 < Q^2 < 0.45\,\mathrm{GeV}^2$ and E_e=500 MeV. The lower panels show relativistic cross sections summed over the phase-space regions defined additionally by a finite p_{miss} bin and labelled by the bin position for two bin widths: 0.05 GeV (a) and 0.025 GeV (b) obtained with the plane wave impulse approximation (dotted lines) and performing the *full* calculations (solid lines).

2. *Polarization observables in the "$Q^2 - p_{miss}$" kinematics*

Also polarization observables discussed in Refs. [53, 54] can be studied in the "$Q^2 - p_{miss}$" kinematics or be summed over any part of the available phase space. However, if we want to use exactly the same kinematics as for the cross section, where we integrate over the azimuthal angle Φ_p, then $\langle A_d^V \rangle = \langle A_{ed}^T \rangle = 0$. It means that some other kinematics has to be chosen to study these two observables, which additionally vanish under the plane wave impulse approximation.

Thus we restrict ourselves to the remaining two: A_d^T and A_{ed}^V. They are not just summed as it was the case for the cross sections but weighted with the (unpolarized) cross section calculated at the same points of the considered phase-space domain. Since these observables

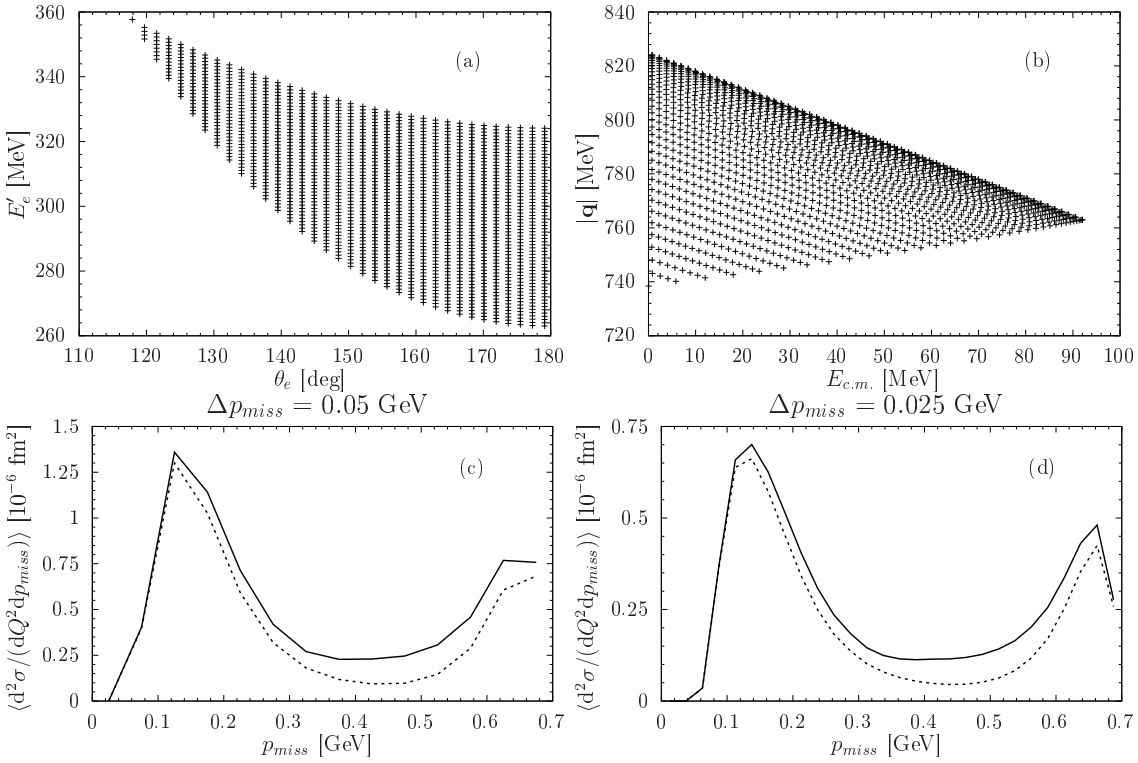

FIG. 23. The same as in Fig. 22 for $0.525\,\mathrm{GeV}^2 < Q^2 < 0.675\,\mathrm{GeV}^2$.

are defined for a given deuteron polarization axis, we choose this time the deuteron polarization axis parallel and perpendicular to the three-momentum transfer $\mathbf{q}$. Since the results do not change significantly with Δp_{miss}, we display them in Figs. 24 and 25 only for $\Delta p_{miss} = 0.025$ GeV. Our *plane wave* and *full* predictions are quite different in the middle of the p_{miss} intervals but come close together otherwise. Thus these two observables can provide more information about the final state interaction effects than the unpolarized cross sections.

G. Neutrino reactions with the deuteron

There also many reactions induced by neutrinos or antineutrinos. We start with predictions for the elastic NC $\nu + d \to \nu + d$ total cross section. They are obtained both in the laboratory and in the CM frame. We expect some deviations between these two predictions due to the incomplete current operator. This problem is illustrated in Fig. 26, where we show three predictions for the total cross section in elastic NC driven neutrino-deuteron scattering. The cross section is calculated nonrelativistically in the laboratory frame and relativistically

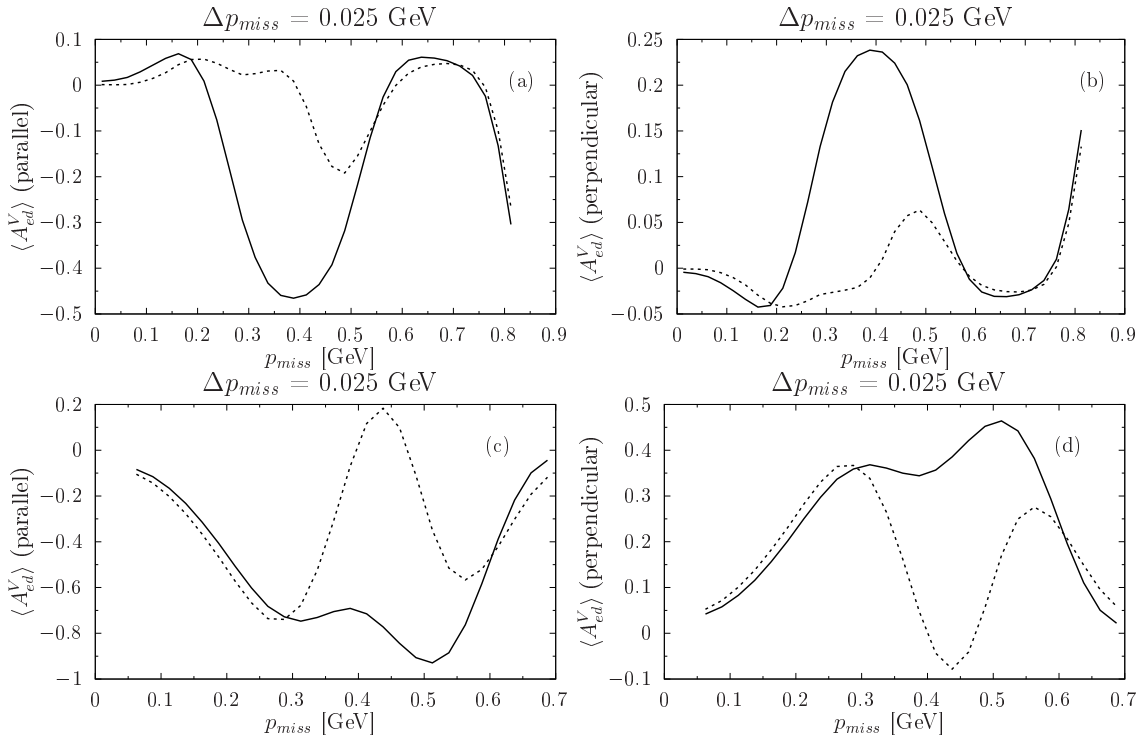

FIG. 24. Averaged theoretical predictions for A_d^T at $0.35\,\mathrm{GeV}^2 < Q^2 < 0.45\,\mathrm{GeV}^2$ ((a) and (b)) and $0.525\,\mathrm{GeV}^2 < Q^2 < 0.675\,\mathrm{GeV}^2$ ((c) and (d)) are shown as a function of the magnitude of the missing momentum p_{miss} for the deuteron polarization axis parallel ((a) and (c)) and perpendicular ((b) and (d)) to the three-momentum transfer $\mathbf{q}$. The *plane wave* (*full*) calculations are represented by the dotted (solid) line.

both, in the laboratory frame and in the total momentum zero frame. Up to approximately $E_\nu^{lab} \leq 500$ MeV all the calculations yield very similar results but the situation changes for higher neutrino energies. Actually the deviation between the two relativistic predictions is larger than the difference between the nonrelativistic and relativistic results obtained in the laboratory frame. It is, however, evident that this observable hides all the differences bound in particular with the difference between the relativistic and nonrelativistic kinematics.

We calculated also breakup cross sections for two selected reactions, $\nu + d \to \nu + p + n$ as well as $\bar{\nu} + d \to e^+ + n + n$.

The formulas for the neutrino induced deuteron breakup reactions are very similar to those for electron scattering. Adjusting Eq. (83), the formula for the total breakup cross

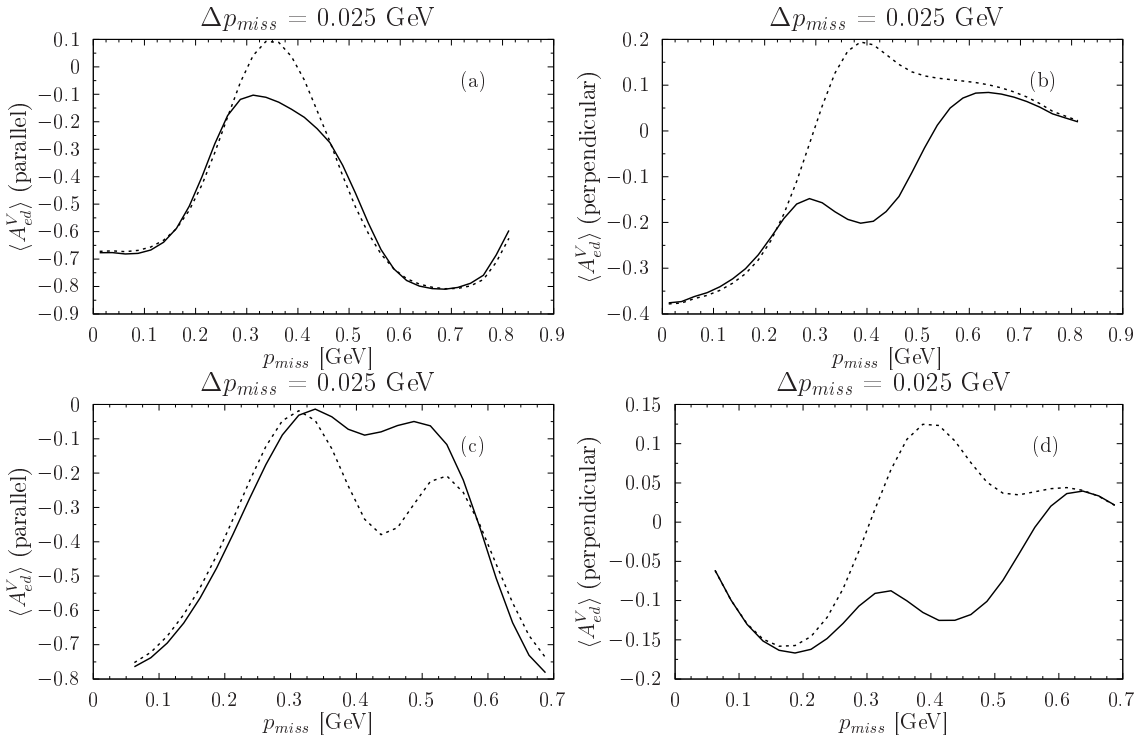

FIG. 25. The same as in Fig. 24 for A_{ed}^V.

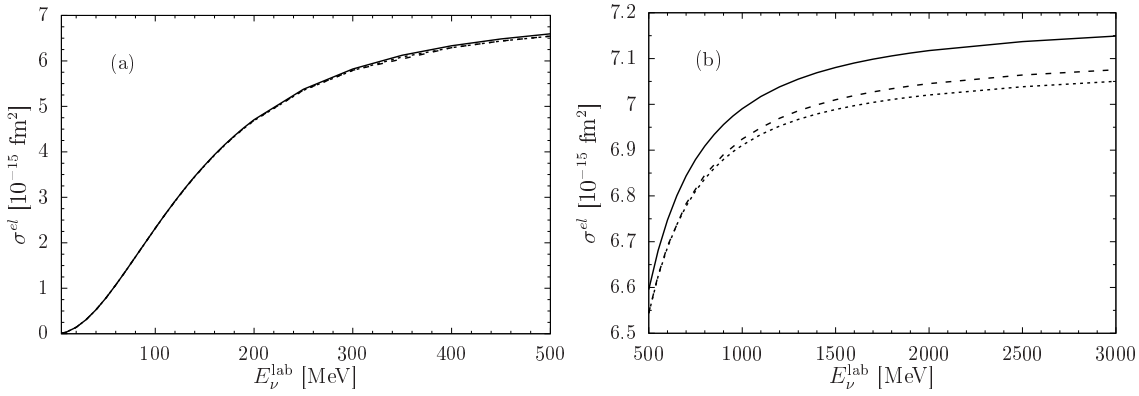

FIG. 26. Predictions for the total elastic cross section $\sigma^{\rm el}$ in neutrino-deuteron scattering shown as a function of the laboratory neutrino energy for neutrino energies E_ν^{lab} (a) smaller and (b) bigger than 500 MeV. The cross was evaluated relativistically in the laboratory system (solid line) and in the center of mass system (dotted line), as well as non-relativistically in the laboratory system (dashed line).

section is

$$\sigma^{br} = \int \mathrm{d}\hat{\mathbf{p}}'_\nu \int_0^{|\mathbf{p}'_\nu|^{max}} \mathrm{d}|\mathbf{p}'_\nu| \, \frac{\mathrm{d}^3\sigma}{\mathrm{d}\hat{\mathbf{p}}'_\nu \mathrm{d}|\mathbf{p}'_\nu|}$$
$$= 2\pi \int_0^\pi \mathrm{d}\theta_{p'_\nu} \sin\theta_{p'_\nu} \int_0^{|\mathbf{p}'_\nu|^{max}} \mathrm{d}|\mathbf{p}'_\nu| \, \frac{\mathrm{d}^3\sigma}{\mathrm{d}\hat{\mathbf{p}}'_\nu \mathrm{d}|\mathbf{p}'_\nu|}\Big|_{\phi_{p'_\nu}=0} . \quad (103)$$

We also mention that for the $\bar{\nu}_e + d \to e^+ + n + n$ charged-current driven reaction the single-nucleon weak current operator assumes a well-known form

$$\langle \mathbf{p}', \mu', \tau' | \, J^\mu_{k,\mathrm{WCC}}(0) \, | \mathbf{p}, \mu, \tau \rangle$$
$$= \delta_{\tau'-1/2} \, \delta_{\tau 1/2} \, \bar{u}(\mathbf{p}', \mu') \left(F_1^C(Q^2)\gamma^\mu + \frac{i}{2m}\sigma^{\mu\nu} q_\nu F_2^C(Q^2) \right.$$
$$\left. + F_A^C(Q^2)\gamma^\mu\gamma_5 + \frac{q^\mu}{m}\gamma_5 F_P^C(Q^2) \right) u(\mathbf{p}, \mu) \, , \quad (104)$$

with the weak charged-current nucleon form factors F_i^C. For recent parametrizations of these quantities see for example [9, 12]. The cross section formulas for this reaction have to be additionally multiplied by $\cos^2\theta_C$, where $\theta_C \approx 13^\circ$ is the Cabibbo angle and the correction factor due to two identical particles in the final state has to be introduced.

In Fig. 27 we display relativistic and nonrelativistic predictions with (*full*) and without (*plane wave*) the rescattering contribution in the nuclear matrix elements and additionally two nonrelativistic predictions, where the nonrelativistic single-nucleon current operator is augmented by relativistic $(p/m)^2$ corrections. Strictly spoken, our way of introducing rescattering effects is valid only for the center of mass energies smaller than the pion mass, so the *full* results should be treated with great care. We see, however, that these contributions in all the three cases are small. Adding the corrections to the nonrelativistic current operator makes the difference between the nonrelativistic and relativistic predictions bigger for the NC induced reaction but brings the "corrected" nonrelativistic results closer to the relativistic predictions for the CC driven process.

The total breakup cross section is obtained as a result of angular integration over the whole solid angle corresponding to the final lepton momentum. In Fig. 28 we show the differential breakup cross sections $\mathrm{d}\sigma/\mathrm{d}\hat{\mathbf{p}}'_\nu$ at two different laboratory neutrino energies E_ν= 120 MeV and 700 MeV for the $\nu + d \to \nu + p + n$ process. The angular distributions calculated relativistically and nonrelativistically show only small but visible differences and clearly change with the initial neutrino energy. Also the shape of the angular distribution strongly depends on the initial (anti)neutrino energy. The corresponding results shown in

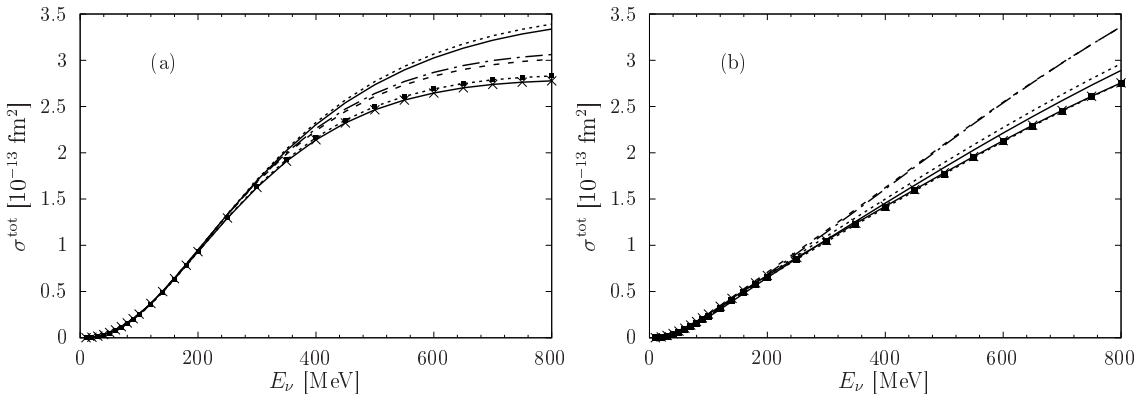

FIG. 27. The *plane wave* and *full* predictions for the total breakup cross section $\sigma^{\rm tot}$ for the (a) $\nu + d \to \nu + p + n$ and (b) $\bar{\nu} + d \to e^+ + n + n$ reaction as a function of the initial (anti)neutrino laboratory energy E_ν. The solid (dotted) line represents the differential cross section with (without) the contribution of the rescattering term calculated relativistically. The dashed (dash-dotted) line represents the differential cross section with (without) the contribution of the rescattering term and calculated within the non-relativistic treatment. The solid (dashed) line with white (black) squares represents the result for the non-relativistic calculations with (without) the contribution of the rescattering term and with the $(p/m)^2$ corrections to the nonrelativistic single-nucleon current operator.

Fig. 29 for the $\bar{\nu} + d \to e^+ + n + n$ reaction are different, especially for the lower energy, where for the NC reaction no peak at forward angles is observed. The peak visible for both reactions at the higher energy is broader in the case of the NC induced reaction. The relativistic features are more pronounced in the case of the CC driven process.

V. SUMMARY AND OUTLOOK

We give a complete relativistic formalism and construct tools to perform calculations of exclusive, semi-exclusive and inclusive unpolarized cross sections and various polarization observables in electron and neutrino scattering experiments with deuteron targets. In the present work the strong interaction dynamics is defined by an explicit dynamical unitary representation of the Poincaré group[1]. In the chosen framework representations of space translations and rotations in the interacting and non-interacting representations are identical

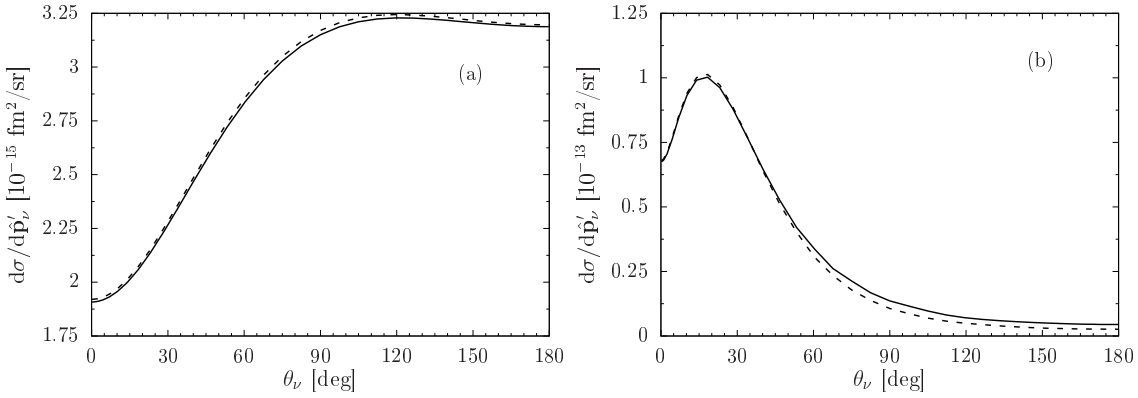

FIG. 28. The differential breakup cross section $d\sigma/d\hat{\mathbf{p}}'_\nu$ for the $\nu+d \to \nu+p+n$ process calculated in the laboratory frame for the initial neutrino energies E_ν= 120 MeV (left panel) and 700 MeV (right panel). The lines are the same as in Fig. 26.

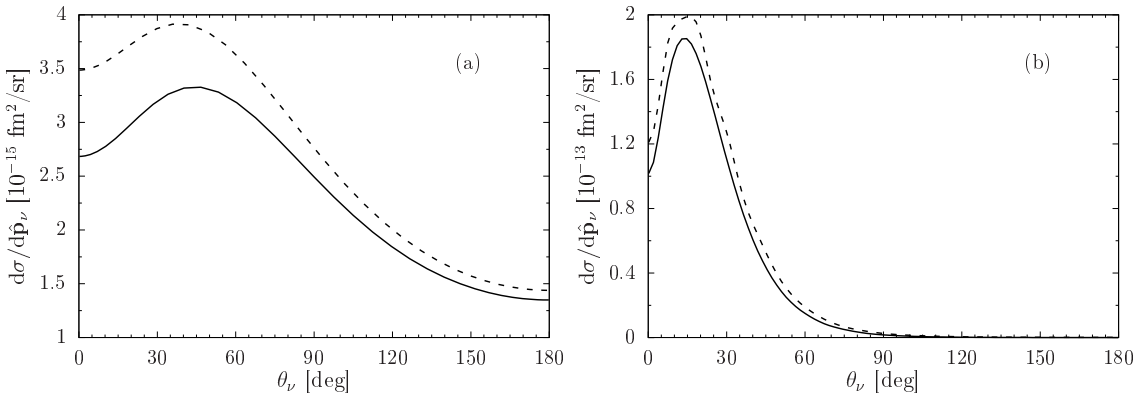

FIG. 29. Same as Fig. 28, but for the $\bar{\nu} + d \to e^+ + n + n$ process.

[4]. The Argonne V18 potential [3] is the starting point for building the relativistic nucleon-nucleon interaction reproducing the experimental deuteron binding energy and nucleon-nucleon scattering observables [2].

Our formalism does not take into account the pion production channel and neglects two-body contributions in the electromagnetic as well as in the weak nuclear current operator. These limitations require additional studies and will be addressed in subsequent investigations. Presently the description of the deuteron form factor $B(Q^2)$ and the deuteron tensor analyzing power T_{20} suggest the need for two-body contributions to the current. The current model is best applicable to kinematics, where the internal two-nucleon energy remains

below the pion production threshold but the magnitude of the three-momentum transfer extends at least to several GeV. Here the final-state nucleon-nucleon interactions can be included exactly. In particular we demonstrate fair agreement with the experimental data for deuteron electrodisintegration in the region of quasi-elastic peak, where the dynamics is governed predominantly by the single-nucleon current operator. Our predictions for the total cross sections in the neutral-current and charged-current induced reactions are also quite reliable, since the two-nucleon contributions in these reactions were shown not to be strong [12]. We demonstrate that the use of the relativistic kinematics is mandatory for the magnitudes of the three-momentum transfer comparable and higher than the nucleon mass. Relativistic $(p/m)^2$ corrections to the nonrelativistic single-nucleon current are to be used with great caution. The fact that purely nonrelativistic and relativistic results for the total elastic neutral-current driven neutrino-deuteron scattering cross section agree very well does not justify the use of the nonrelativistic framework in the relativistic domain, where already the nonrelativistic kinematics is wrong. The frame dependence of our calculations of the total elastic cross section points to a need for corrections due to two-body currents. The predictions obtained in the laboratory frame and in the total momentum zero frame differ at 3 GeV by about 1.5 %, which can be traced back to the inadequacy of our weak nuclear current operator. The kinematics of the electron and neutrino induced deuteron breakup is relatively simple and allows one to easily consider *any* kinematical conditions. We show examples in the so-called "$Q^2 - p_{miss}$" kinematics, making predictions for the unpolarized cross sections and selected polarization observables. We are ready to analyze experimental data and plan to improve the present framework by augmenting it with two-nucleon current contributions. Last not least, the Argonne V18 nucleon-nucleon potential can be replaced by the recently developed accurate chiral interaction [57].

Appendix A: Nuclear current matrix elements

Bearing in mind that we will also need nuclear matrix elements for the deuteron disintegration reactions we actually calculate a chain of matrix elements, starting from

$$\langle \mathbf{p}'_1, \mu'_1, \tau'_1, \mathbf{p}'_2, \mu'_2, \tau'_2 | J^{\mu}_{nuc}(0) | \mathbf{p}_D, \mu_D, D \rangle \, , \tag{A1}$$

then we insert the completeness relations to obtain

$$\begin{aligned}
&\langle \mathbf{p}_1', \mu_1', \tau_1', \mathbf{p}_2', \mu_2', \tau_2' | J^\mu_{nuc}(0) | \mathbf{p}_D, \mu_D, D \rangle \\
&= \sum_{\mu_1\tau_1} \sum_{\mu_2\tau_2} \int \mathrm{d}\mathbf{p}_1 \mathrm{d}\mathbf{p}_2 \langle \mathbf{p}_1', \mu_1', \tau_1', \mathbf{p}_2', \mu_2', \tau_2' | \, J^\mu_{nuc}(0) \, | \mathbf{p}_1, \mu_1, \tau_1, \mathbf{p}_2, \mu_2, \tau_2 \rangle \\
&\quad \times \sum_{jlst\tau\mu} \int \mathrm{d}\mathbf{p} \, \mathrm{d}k \, k^2 \, \langle \mathbf{p}_1, \mu_1, \tau_1, \mathbf{p}_2, \mu_2, \tau_2 | (j,k)\mathbf{p}, \mu; lst\tau \rangle \\
&\quad \times \langle (j,k)\mathbf{p}, \mu; lst\tau | \mathbf{p}_D, \mu_D, D \rangle
\end{aligned} \tag{A2}$$

and, using Eqs. (48) and (54), we arrive at

$$\begin{aligned}
&\langle \mathbf{p}_1', \mu_1', \tau_1', \mathbf{p}_2', \mu_2', \tau_2' | J^\mu_{nuc}(0) | \mathbf{p}_D, \mu_D, D \rangle \\
&= \mathcal{N}^{-1}(\mathbf{p}_1, \mathbf{p}_2') \sum_{\mu_1\tau_1} \langle \mathbf{p}_1', \mu_1', \tau_1' | J^\mu_1(0) | \mathbf{p}_1, \mu_1, \tau_1 \rangle \, (1/2, \tau_1, 1/2, \tau_2' | 0, 0) \\
&\quad \times \sum_{l=0,2} \phi_{D,l}(k) \sum_{\mu_l\mu_s} Y_{l\mu_l}(\hat{\mathbf{k}}) \, (l, \mu_l, 1, \mu_s | 1, \mu_D) \\
&\times \sum_{\mu_1''\mu_2''} (1/2, \mu_1'', 1/2, \mu_2'' | 1, \mu_s) \, D^{1/2}_{\mu_1\mu_1''} \left[R_w \left(\mathbf{p}_D / m_{120}, \mathbf{k} \right) \right] D^{1/2}_{\mu_2'\mu_2''} \left[R_w \left(\mathbf{p}_D / m_{120}, -\mathbf{k} \right) \right] ,
\end{aligned} \tag{A3}$$

where $\mathbf{k} = \mathbf{k}(\mathbf{p}_1, \mathbf{p}_2')$, $k = |\mathbf{k}|$, $\mathbf{p}_1 = \mathbf{p}_D - \mathbf{p}_2$ and $\mathcal{N}(\mathbf{p}_1, \mathbf{p}_2)$ is given in Eq. (50).

For the semi-exclusive observables in the deuteron breakup process, where we integrate over all the nuclear states for the fixed final lepton scattering angle and energy, it is convenient to prepare matrix elements

$$\langle \mathbf{k}', \mathbf{p}', \mu_1', \tau_1', \mu_2', \tau_2' | J^\mu_{nuc}(0) | \mathbf{p}_D, \mu_D, D \rangle \, . \tag{A4}$$

They take the following form

$$\begin{aligned}
&\langle \mathbf{k}', \mathbf{p}', \mu_1', \tau_1', \mu_2', \tau_2' | J^\mu_{nuc}(0) | \mathbf{p}_D, \mu_D, D \rangle \\
&= \sum_{\mu_1''\mu_2''} \int \mathrm{d}\mathbf{p}_1'' \, \mathrm{d}\mathbf{p}_2'' \, \langle \mathbf{k}', \mathbf{p}', \mu_1', \mu_2' | \mathbf{p}_1'', \mu_1'', \mathbf{p}_2'', \mu_2'' \rangle \\
&\quad \times \langle \mathbf{p}_1'', \mu_1'', \tau_1', \mathbf{p}_2'', \mu_2'', \tau_2' | \, J^\mu_{nuc}(0) \, | \mathbf{p}_D, \mu_D, D \rangle \, ,
\end{aligned} \tag{A5}$$

where

$$\begin{aligned}
&\langle \mathbf{k}', \mathbf{p}', \mu_1', \mu_2' | \mathbf{p}_1'', \mu_1'', \mathbf{p}_2'', \mu_2'' \rangle \\
&= \mathcal{N}(\mathbf{p}_1'', \mathbf{p}_2'') \, \delta(\mathbf{p}_1'' - \mathbf{p}_1(\mathbf{k}', \mathbf{p}')) \, \delta(\mathbf{p}_2'' - \mathbf{p}_2(\mathbf{k}', \mathbf{p}')) \\
&\times D^{1/2\,*}_{\mu_1'\mu_1''} \left[R_w \left(\mathbf{p}' / m_{120}', \mathbf{k}' \right) \right] \, D^{1/2\,*}_{\mu_2'\mu_2''} \left[R_w \left(\mathbf{p}' / m_{120}', -\mathbf{k}' \right) \right] \, .
\end{aligned} \tag{A6}$$

The rescattering contributions to the breakup matrix elements are calculated using partial wave states. That requires that also matrix elements

$$\langle (j',k')\mathbf{p}',\mu';l',s';t'\tau'|J^{\mu}_{nuc}(0)|\mathbf{p}_D,\mu_D,D\rangle \tag{A7}$$

are evaluated. These matrix elements are

$$\begin{aligned}
&\langle (j',k')\mathbf{p}',\mu';l',s';t'\tau'|J^{\mu}_{nuc}(0)|\mathbf{p}_D,\mu_D,D\rangle \\
&= \sum_{\mu_1''\mu_2''}\sum_{\tau_1''\tau_2''}\int \mathrm{d}\mathbf{k}\,\mathrm{d}\mathbf{p}\,\langle (j',k')\mathbf{p}',\mu';l',s';t'\tau'|\mathbf{k},\mathbf{p},\mu_1'',\tau_1'',\mu_2'',\tau_2''\rangle \\
&\quad\times\langle \mathbf{k},\mathbf{p},\mu_1'',\tau_1'',\mu_2'',\tau_2''|\,J^{\mu}_1(0)\,|\mathbf{p}_D,\mu_D,D\rangle\,,
\end{aligned} \tag{A8}$$

where

$$\begin{aligned}
&\langle (j',k')\mathbf{p}',\mu';l',s';t'\tau'|\mathbf{k},\mathbf{p},\mu_1'',\tau_1'',\mu_2'',\tau_2''\rangle \\
&= \delta(\mathbf{p}'-\mathbf{p})\,\frac{\delta(k-k')}{k^2}\,(1/2,\tau_1'',1/2,\tau_2''|t',\tau') \\
&\times\sum_{\mu_l'\mu_s'}(l',\mu_l',s',\mu_s'|j',\mu')\;(1/2,\mu_1'',1/2,\mu_2''|s',\mu_s')\;Y^*_{l'\mu_l'}(\hat{\mathbf{k}}')\,.
\end{aligned} \tag{A9}$$

The result for matrix elements (A7) can be also used to easily calculate nuclear matrix elements for the elastic scattering reactions, since

$$\begin{aligned}
&\langle \mathbf{p}'_D,\mu'_D,D|J^{\mu}_{nuc}(0)|\mathbf{p}_D,\mu_D,D\rangle \\
&= \int \mathrm{d}\mathbf{p}'\sum_{l'=0,2}\int \mathrm{d}k'k'^2\,\langle \mathbf{p}'_D,\mu'_D,D|(1,k')\mathbf{p}',\mu';l',1;00\rangle \\
&\quad\times\langle (1,k')\mathbf{p}',\mu';l',1;00|J^{\mu}_{nuc}(0)|\mathbf{p}_D,\mu_D,D\rangle \\
&= \sum_{l'=0,2}\int \mathrm{d}k'k'^2\,\phi_{D,l'}(k')\,\langle (1,k')\mathbf{p}'_D,\mu'_D;l',1;00|J^{\mu}_{nuc}(0)|\mathbf{p}_D,\mu_D,D\rangle\,.
\end{aligned} \tag{A10}$$

The rescattering part (90) of the ${}^{(-)}\langle \mathbf{p}'_1,\mu'_1,\tau'_1,\mathbf{p}'_2,\mu'_2,\tau'_2|J^{\mu}_{nuc,EM}(0)|\mathbf{p}_D,\mu_D,D\rangle$ matrix element is calculated in two steps. We calculate first

$$\begin{aligned}
&\langle (j',k')\mathbf{p}',\mu';l's't'\tau'|\,t(E+i\epsilon)G_0(E+i\epsilon)\,J^{\mu}_{nuc}(0)\,|\mathbf{p}_D\mu_D D\rangle \\
&= \sum_{j\mu lst\tau}\int \mathrm{d}\mathbf{p}\int \mathrm{d}k\,k^2\,\langle (j',k')\mathbf{p}',\mu';l's't'\tau'|\,t(E+i\epsilon)G_0(E+i\epsilon)\;|(j,k)\mathbf{p},\mu;lst\tau\rangle \\
&\quad\times\langle (j,k)\mathbf{p},\mu;lst\tau|\,J^{\mu}_{nuc}(0)\,|\mathbf{p}_D,\mu_D,D\rangle\,,
\end{aligned} \tag{A11}$$

where

$$\begin{aligned}
&\langle (j',k')\mathbf{p}',\mu';l's't'\tau'|\,t(E+i\epsilon)G_0(E+i\epsilon)\;|(j,k)\mathbf{p},\mu;lst\tau\rangle \\
&= \delta(\mathbf{p}'-\mathbf{p})\delta_{jj'}\delta_{\mu\mu'}\delta_{ss'}\delta_{tt'}\delta_{\tau\tau'} \\
&\times\frac{\langle (jk')\mu';l's't'\tau'|\,t(E+i\epsilon,p')\,|(jk)\mu;lst\tau\rangle}{E+i\epsilon-\sqrt{4(m^2+k^2)+|\mathbf{p}'|^2}}
\end{aligned} \tag{A12}$$

and obtain

$$\begin{aligned}
&\langle (j',k')\mathbf{p}',\mu';l's't'\tau'|\, t(E+i\epsilon)G_0(E+i\epsilon)\, J^\mu_{nuc}(0)\,|\mathbf{p}_D,\mu_D,D\rangle \\
&= \sum_l \int \mathrm{d}k\, k^2\, \frac{\langle (j',k'),\mu';l's't'\tau'|\, t(E+i\epsilon,p')\,|(j',k),\mu';ls't'\tau'\rangle}{E+i\epsilon-\sqrt{4(m^2+k^2)+|\mathbf{p}'|^2}} \\
&\qquad \times \langle (j',k)\mathbf{p}',\mu';ls't'\tau'|\, J^\mu_{nuc}(0)\,|\mathbf{p}_D,\mu_D,D\rangle\,. \qquad \text{(A13)}
\end{aligned}$$

The pole in (A13) is treated by dividing and multiplying the integrand by

$$h(E,|\mathbf{p}'|\,,k) \equiv \frac{1}{4}(E+\sqrt{4(m^2+k^2)+\mathbf{p}'^2})\,,$$

which leads to

$$\begin{aligned}
&\langle (j',k')\mathbf{p}',\mu';l's't'\tau'|\, t(E+i\epsilon)G_0(E+i\epsilon)\, J^\mu_{nuc}(0)\,|\mathbf{p}_D,\mu_D,D\rangle \\
&\qquad = m\sum_l \int \mathrm{d}k\, k^2\, h(E,|\mathbf{p}'|\,,k) \\
&\qquad \times \frac{\langle (j',k'),\mu';l's't'\tau'|\, t(E+i\epsilon,p')\,|(j',k),\mu';ls't'\tau'\rangle}{k_0^2-k^2+i\epsilon} \\
&\qquad \times \langle (j',k)\mathbf{p}',\mu';ls't'\tau'|\, J^\mu_{nuc}(0)\,|\mathbf{p}_D,\mu_D,D\rangle\,, \qquad \text{(A14)}
\end{aligned}$$

where

$$k_0 = \frac{1}{2}\sqrt{E^2-|\mathbf{p}'|^2-4m^2}\,. \qquad \text{(A15)}$$

The resulting integral is calculated using standard subtraction techniques.

The result prepared in Eq. (A14) for

$$\langle (j',k')\mathbf{p}',\mu';l's't'\tau'|\, t(E+i\epsilon)G_0(E+i\epsilon)\, J^\mu_{nuc}(0)\,|\mathbf{p}_D,\mu_D,D\rangle$$

together with the two overlaps given in Eqs. (48) and (A9) can be used to calculate the final nuclear matrix elements

$$\langle \mathbf{p}'_1,\mu'_1,\tau'_1,\mathbf{p}'_2,\mu'_2,\tau'_2|\, t(E+i\epsilon)G_0(E+i\epsilon)\, J^\mu_{nuc}(0)\,|\mathbf{p}_D,\mu_D,D\rangle$$

and

$$\langle \mathbf{k}',\mathbf{p}',\mu'_1,\tau'_1,\mu'_2,\tau'_2|\, t(E+i\epsilon)G_0(E+i\epsilon)\, J^\mu_{nuc}(0)\,|\mathbf{p}_D,\mu_D,D\rangle\,,$$

which are needed for the exclusive and semi-exclusive (and eventually total for neutrino induced reactions) cross sections.

ACKNOWLEDGMENTS

One of the authors (J.G.) gratefully acknowledges the financial support of the JSPS International Fellowships for Research in Japan (ID=S19149). One of the authors (W.P.) gratefully acknowledges support of this research by the US Department of Energy, Office of Science, grant number DE-SC0016457. The numerical calculations were partly performed on the supercomputers of the JSC, Jülich, Germany.

---

[1] E. P. Wigner, Ann. Math. **40**, 149 (1939).

[2] H. Kamada and W. Glöckle, Phys. Lett. B **655**, 119 (2007).

[3] R. B. Wiringa, V. G. J. Stoks, and R. Schiavilla, Phys. Rev. C **51**, 38 (1995).

[4] B. Bakamjian and L. H. Thomas, Phys. Rev. **92**, 1300 (1953).

[5] J. D. Bjorken and S. D. Drell, *Relativistic quantum mechanics*, International series in pure and applied physics (McGraw-Hill, New York, NY, 1964).

[6] P. Moussa and R. Stora, *Lectures in Theoretical Physics Vol. VIIA* (McGraw-Hill, University of Colorado Press, 1965).

[7] F. Coester, Helv. Phys. Acta **38**, 7 (1965).

[8] B. D. Keister and W. N. Polyzou, Adv. Nucl. Phys. **20**, 225 (1991).

[9] H. Budd, A. Bodek, and J. Arrington, arXiv:hep-ex/0308005v2 (2003).

[10] J. J. Kelly, Phys. Rev. C **70**, 068202 (2004).

[11] E. L. Lomon, Phys. Rev. C **66**, 045501 (2002).

[12] G. Shen, L. E. Marcucci, J. Carlson, S. Gandolfi, and R. Schiavilla, Phys. Rev. C **86**, 035503 (2012).

[13] T. Donnelly and A. Raskin, Ann. Phys. **169**, 247 (1986).

[14] F. Coester and A. Ostebee, Phys. Rev. C **11**, 1836 (1975).

[15] Y. Huang and W. N. Polyzou, Phys. Rev. C **80**, 025503 (2009).

[16] A. A. Filin *et al.*, Phys. Rev. C **103**, 024313 (2021).

[17] M. N. Rosenbluth, Phys. Rev. **79**, 615 (1950).

[18] M. I. Haftel, L. Mathelitsch, and H. F. K. Zingl, Phys. Rev. C **22**, 1285 (1980).

[19] T. Kolar *et al.*, Phys. Lett. B **824**, 136798 (2022).

[20] H. Witała *et al.*, Phys. Rev. C **77**, 034004 (2008).

[21] J. Golak *et al.*, Phys. Rep. **415**, 89 (2005).

[22] H. Arenhövel, W. Leidemann, and E. L. Tomusiak, Eur. Phys. J. A **23**, 147 (2005).

[23] A. F. Krutov and V. E. Troitsky, Phys. Rev. C **75**, 014001 (2007).

[24] E. Epelbaum, A. M. Gasparyan, J. Gegelia, and M. R. Schindler, Eur. Phys. J. A **50**, 51 (2014).

[25] M. Walzl and U.-G. Meißner, Phys. Lett. B **513**, 37 (2001).

[26] D. Benaksas, D. Drickey, and D. Frèrejacque, Phys. Rev. **148**, 1327 (1966).

[27] R. Berard *et al.*, Phys. Lett. B **47**, 355 (1973).

[28] S. Auffret *et al.*, Phys. Rev. Lett. **54**, 649 (1985).

[29] G. Simon, C. Schmitt, and V. Walther, Nucl. Phys. A **364**, 285 (1981).

[30] C. D. Buchanan and M. R. Yearian, Phys. Rev. Lett. **15**, 303 (1965).

[31] J. E. Elias *et al.*, Phys. Rev. **177**, 2075 (1969).

[32] R. G. Arnold *et al.*, Phys. Rev. Lett. **35**, 776 (1975).

[33] S. Platchkov *et al.*, Nucl. Phys. A **510**, 740 (1990).

[34] S. Galster *et al.*, Nucl. Phys. B **32**, 221 (1971).

[35] R. Cramer *et al.*, Zeitschrift für Physik C Particles and Fields **29**, 513 (1985).

[36] D. Abbott *et al.*, Phys. Rev. Lett. **82**, 1379 (1999).

[37] L. C. Alexa *et al.*, Phys. Rev. Lett. **82**, 1374 (1999).

[38] P. E. Bosted *et al.*, Phys. Rev. C **42**, 38 (1990).

[39] F. Martin *et al.*, Phys. Rev. Lett. **38**, 1320 (1977).

[40] V. Dmitriev *et al.*, Phys. Lett. B **157**, 143 (1985).

[41] B. B. Voitsekhovskii *et al.*, JETP Lett. **43**, 733 (1985).

[42] R. Gilman *et al.*, Phys. Rev. Lett. **65**, 1733 (1990).

[43] M. E. Schulze *et al.*, Phys. Rev. Lett. **52**, 597 (1984).

[44] I. The *et al.*, Phys. Rev. Lett. **67**, 173 (1991).

[45] D. Abbott *et al.*, Phys. Rev. Lett. **84**, 5053 (2000).

[46] P. von Neumann-Cosel *et al.*, Phys. Rev. Lett. **88**, 202304 (2002).

[47] J. Golak *et al.*, Phys. Rev. C **98**, 015501 (2018).

[48] J. Golak *et al.*, Phys. Rev. C **100**, 064003 (2019).

[49] K. M. Hanson *et al.*, Phys. Rev. D **8**, 753 (1973).

[50] S. Rock *et al.*, Phys. Rev. D **46**, 24 (1992).

[51] S. Rock, SLAC-PUB-5239 (1991).

[52] B. P. Quinn *et al.*, Phys. Rev. C **37**, 1609 (1988).

[53] S. Jeschonnek and J. W. Van Orden, Phys. Rev. C **80**, 054001 (2009).

[54] M. Mayer *et al.*, Phys. Rev. C **95**, 024005 (2017).

[55] I. Passchier *et al.*, Phys. Rev. Lett. **88**, 102302 (2002).

[56] K. S. Egiyan *et al.*, Phys. Rev. Lett. **98**, 262502 (2007).

[57] P. Reinert, H. Krebs, and E. Epelbaum, Eur. Phys. J. A **54**, 86 (2018).